UNIVERSITY OF CALIFORNIA, SAN DIEGO

Novel graphene production: an aqueous arc discharge process

A dissertation submitted in partial satisfaction of the requirements for the degree Doctor of Philosophy

in

Materials Science and Engineering

by

Sejung Kim

Committee in charge:

Professor Michael J. Heller, Chair
Professor Kenneth J. Vecchio, Co-Chair
Professor Yeshaiahu Fainman
Professor Darren J. Lipomi
Professor Donald J. Sirbuly

2015

The Dissertation of Sejung Kim is approved, and it is acceptable in quality and form for publication on microfilm and electronically:

_____

_____

_____

_____
Co-Chair

_____
Chair

University of California, San Diego

2015

Dedication

Dedicated to my loving wife Soojin and my big family

Who have always shown love and support

Table of Contents

List of Figures

Acknowledgements

During my graduate studies at University of California at San Diego, I have been blessed to meet so many talented people. Firstly, I would like to thank my advisor enough for being my mentor; I would like to express my sincerest gratitude to Professor Michael J. Heller for giving me a wonderful opportunity to be part of the greatest journey that I have experienced thus far. His encouragement, guidance, and passion for science always inspire me to joyfully follow my own trail without any hesitation.

I would like to thank my committee members, Prof. Kenneth J. Vecchio as my co-advisor, Prof. Yeshaiahu Fainman, Prof. Donald J. Sirbuly, and Darren J. Lipomi for helpful discussion and suggestions on my dissertation.

I am indebted to all my former and present members of the Heller group who are my colleagues as well as good friend of mine. In particular, I am truly grateful to Dr. Youngjun Song and Dr. Tsukasa Takahashi for being a dependable friend and giving me a valuable discussion and encouragement. Many thanks to Dr. Jennifer Marciniak and Dr. Stuart Ibsen for getting me involved in exosome DEP research. Without their help, I would not have been able to succeed.

Lastly, I would like to express my deepest gratitude and love to my wife, Soojin Kim, and my mother, Sun-Nam Hong, and my big family: Hyun-Joong Kim, Hyo-Joong Kim, Won-Joong Kim, Dae-Joong Kim, Jung-Hwa Kim, Bok-Ee Kim, Min-Im Um, Kyung-Sik Kim, Mi-Ran Lee, Soo-Hyun Kim, Sung-Eun Kim, Jong-Hoon Kim, and my little stars: Seo-Young Kim, Seo-Yoon Kim, Joon-Seo Kim, Tae-Wan Kim, Dong-Wan Kim, Joo-Wan Kim, Do-Keon Kim, Do-Yoon Kim, Do-Young Kim, Do-Hu Kim, Ha-

Yoon Kim and unborn kid.

Chapter 1, in full, is an introductory material as the outline of this thesis and the importance of this research.

Chapter 2, in full, is an overview of the synthetic methods as the bottom line of the research.

Chapter 3, in part, is currently being submitted for publication of the material. Kim, Sejung; Song, Youngjun; Marciniak, Jennifer; Heller, Michael J. The dissertation author was the primary investigator and author of this material.

Chapter 4, in part, is currently being submitted for publication of the material. Kim, Sejung; Song, Youngjun; Marciniak, Jennifer; Heller, Michael J. The dissertation author was the primary investigator and author of this material.

Chapter 5, in full, is currently being prepared for submission for publication of the material. Kim, Sejung; Song, Youngjun; Marciniak, Jennifer; Ko, Se-Yoen; Heller, Michael J. The dissertation author was the primary investigator and author of this material.

Chapter 6, in full, is a reprint of the material as it accepted in Small, 2015. Kim, Sejung; Song, Youngjun; Takahashi, Tsukada; Oh, Taeseok; Heller, Michael J. The dissertation author was the primary investigator and author of this material.

Vita

2007	Bachelor of Science in Chemical Engineering
	Chonbuk National University, Korea
2009	Master of Science in Chemical Engineering
	Chonbuk National University, Korea
2008-2009	Korea Basic Science Institute, Korea
2015	Doctor of Philosophy in Materials Science and Engineering
	University of California San Diego, USA

Publications

[1] **Sejung Kim**, Youngjun Song, Tsukasa Takahashi, Taesoek Oh, Michael J. Heller, An aqueous single reactor arc discharge process for the synthesis of graphene nanospheres. Small. 2015;11:5041-5046.

[2] **Sejung Kim**, Youngjun Song, Jennifer Wright, Michael J. Heller, Graphene bi- and trilayers produced by a novel aqueous arc discharge process, submitted to Carbon.

[3] **Sejung Kim**, Youngjun Song, Jennifer Wright, SeoYeon Ko, Michael J. Heller, Nanoporous graphene filters for water purification created by an aqueous arc discharge process. (*manuscript in preparation*)

ABSTRACT OF THE DISSERTATION

Novel graphene production: an aqueous arc discharge process

by

Sejung Kim

Doctor of Philosophy in Materials Science and Engineering

University of California, San Diego, 2015

Professor Michael J. Heller, Chair

Professor Kenneth J. Vecchio, Co-Chair

Graphene plays important roles in technological developments regarding electronic device, environment and energy management and the motivation to prepare two-dimensional (2D) nanomaterials. As the pioneer for 2D nanomaterials, graphene has been shown to be not only thermodynamically stable, but also superior in terms of electronic and mechanical properties and that it can be processed into a wide variety of novel

materials. However, they are still limited to the challenges such as multi-stacked layers and low efficiency towards a scalable and cost-effective manufacturing process.

In this dissertation, we develop an aqueous arc discharge process as a novel method to produce graphene. This novel graphene production process has the following features: (1) Low energy power consumption process to exfoliate graphene from graphite rather than to evaporate carbon molecules. (2) Water used as a dielectric medium uses a coolant to maintain the temperature during the process. (3) Controllable graphene layers and the number of oxygen-related functional groups. (4) A seamless process for morphological transition of graphene from 2D to three-dimensional (3D) construction.

The graphene produced by our aqueous arc discharge is investigated as transparent electrodes and water desalination membranes. For the transparent electrodes, bi- and trilayers of graphene are adopted to be at high electrical conductance and transmittance, which are collected by vacuum-assisted filtration and then transferred to a flexible transparent polymer films. In the case of the application for water desalination, the effect of the degree of graphene oxidation is investigated and found that the affinity of 2D nanochannels to water molecules and ions affected to the flow rate and salt rejection rate due to the interfacial friction at the interface.

The seamless process of the aqueous arc discharge has been achieved to crumple 2D graphene into 3D graphene nanospheres with the controllable degree of crumpling of graphene. The formation of oil-in-water emulsion during arc discharge can entrap and crumple the exfoliated graphene, simultaneously. The degree of graphene deformation can be controlled by adjusting the flow rate of oil into the plasma zone.

Chapter 1: Introduction

1.1 Introduction

The discovery of graphene, a two-dimensional (2D) hexagonal lattice composed of sp^2-hybridized carbon atoms, leads to the intensive investigation of the 2D nanostructures for various scientific and technological research achievements.[1-6] Graphene was regarded as the raw materials for multi-dimensional graphitic nanostructures due to its thermodynamic instability: graphene can be wrapped up into 0D (fullerene) and be rolled into 1D (carbon nanotubes). Otherwise, it can be stacked up into 3D bulk materials (graphite).[7] Since the first isolation of graphene from the graphite by scotch tape method, it has been found to have the Quantum Hall Effect (QHE) and a unique band structure, which leads to the investigation for the post generation to alternate Si-based transistors, because it has high charge carrier mobility ($> 2 \times 10^5$ cm^2 V^{-1} s^{-1} at an electron density of 2×10^{11} cm^{-2}).[8] In addition, graphene was found to have high thermal conductivity (over 3000 W mK^{-1}), remarkably high Young's modulus (> 0.5 – 1 TPa), [9] and high surface area (> 2500 m^2 g^{-1}).[10] The exceptional properties of graphene make intensive investigation for many applications such as energy storage, catalyst, biological labeling, and flexible electronics. [11-16]

1.1.1 Brief history of graphene

The production of graphene was started from the exfoliation of graphite oxide (GO), and graphite intercalation compounds (GICs). Currently, the manipulation of GO

can prepare the reduced graphene oxide (r-GO), which can be considered as the precursor of graphene.

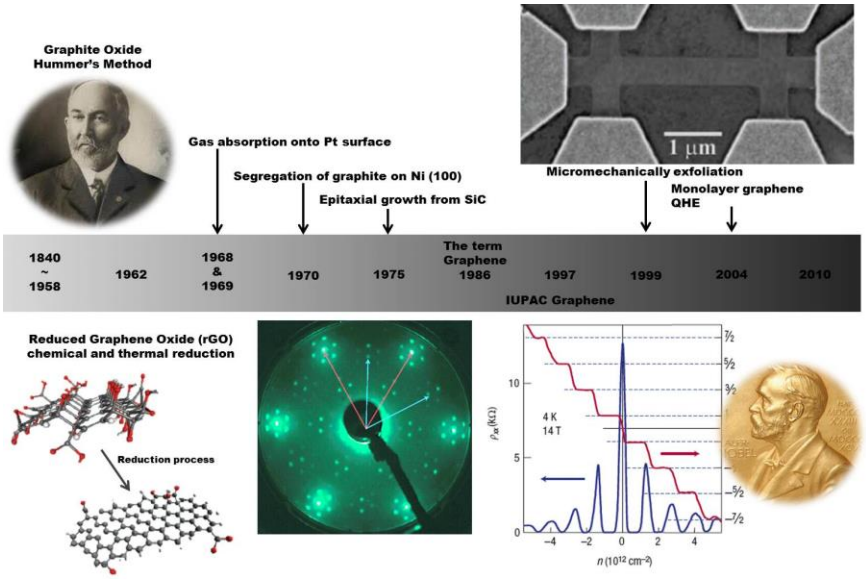

Figure 1.1 A timeline of selected events in the history of graphene for its preparation, isolation and characterization.

As demonstrated in **Figure 1. 1**, the chemical process of conversion of graphite into graphite oxide started from 1840 by a German scientist Schafhaeutl who developed the intercalation and exfoliation of graphite with strong acids such as sulfuric acid and nitric acids. [5] Basically, the interlayer distance is widened by inserting small molecules or oxygen on the basal planes. Since then, various types of intercalants and exfoliants have been used, including alkali metals, transition metals, fluoride salts and organic species. Later, Hummer's method was developed in 1958 by using concentrated sulfuric acid, sodium nitrate and potassium permanganate towards a safer, faster and more

efficient method.[5] In 1962, Boehm et al. developed the chemical and thermal reduction process of graphene oxide. Later, the mono- and multi-layered graphite on metal surface were found by gas absorption on the Pt (100) surface or segregation of graphite on the Ni(100) surface. In 1975, van Bommel et al. described that monolayer of graphite was obtained from single crystals of silicon carbide at elevated temperatures under ultrahigh vacuum (< 10^{-10} Torr). The term graphene was first named by Boehm et al. in 1986 and IUPAC recommended terminology for the description as "graphene layer is a single carbon layer of the graphite structure, describing its nature by analogy to a polycyclic aromatic hydrocarbon of quasi infinite size". In 1999, Ruoff et al. developed a micromechanical process that was combined with oxygen-plasma etching to lithographic patterning of highly ordered pyrolytic graphite (HOPG). [5]

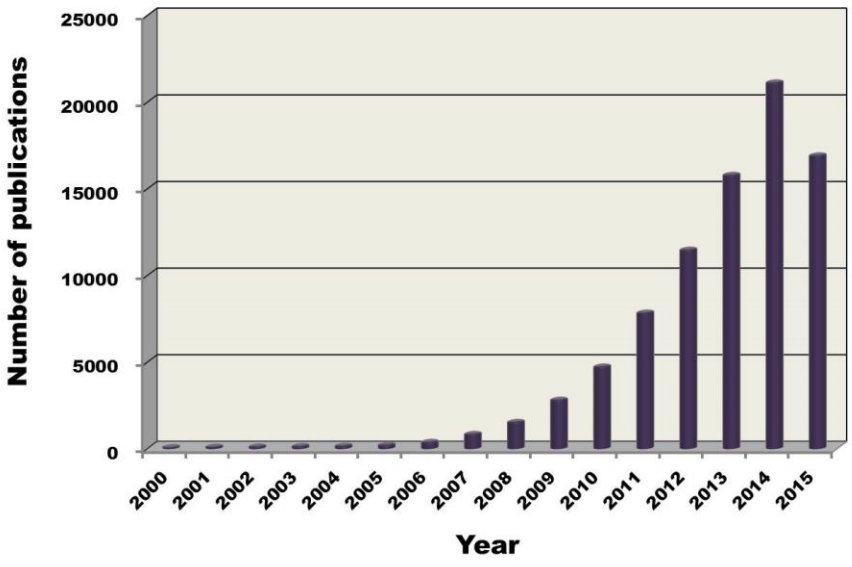

Figure 1.2 Publications on graphene from 2000 to Sept. 2015. Source ISI Web of Science (search Topic: Graphene). Publications on graphene prior to 2000 are not plotted.

Geim, Novoselov demonstrated that this mechanical approach could produce thin graphite flakes and 0.8 nm thick of graphene on SiO_2 surface, which were visualized by the optical microscopy and their electric-field effect was demonstrated. [1,2] Nowadays, chemical vapor deposition (CVD) on metal surfaces for producing graphene has been optimized and has become a major technique to produce graphene. The studies of graphene including the control of the graphene layers, functionalization, and applications of graphene have grown exponentially as shown in **Figure 1.2**.

1.1.2 Optoelectrical properties

According to Fresnel equations, the theoretical transmittance (T) of a free standing graphene can be written, [17]

$$T = (1 + 0.5\ n\alpha)^{-2} = 1 - n\alpha = 97.7\%$$

where α is the fine structure constant, $\alpha = e^2/\hbar\ c = 1/137$. The absorbance can be calculated as $A = 1 - T = \pi\alpha = 2.3\%$. In the visible region, the incident light is reflected less than 0.1% by graphene, thus the optical absorption of graphene layers can be proportionally increased by 2.3% according to the number of layers. [7,17] The mechanically exfoliated graphene has the transmittance of 97.7%, which is in excellent agreement with the theoretical study for its defect-free sp^2 structure. In addition, graphene synthesized by chemical vapor deposition (CVD) shows similar optical transmittance (97.4%).[18] In both the case of the mechanically exfoliated graphene and the CVD graphene, the transmittance linearly decreases as the number of layers is increased, which demonstrates that the transmittance of the graphene films highly depends on their crystal

quality during the synthetic process.

In addition to the transmittance, in general, the resistance of graphene-based films highly depends on their surface structure and crystal quality, which are variable according to the different film fabrication methods. In the case of thermally reduced graphene oxide (GO), the transmittance is much higher than that of the pristine graphene (defect-free) due to the presence of defects, but yields to high sheet resistance due to its poor crystal quality. Another approach to produce more conductive graphene-based films is using liquid-based exfoliation of graphene, which results in the sheet resistance of 5 $k\Omega/cm^2$ with a transmittance of 90%.[18] However, the exfoliation-based graphene shows the high sheet resistance due to the non-uniformity of the graphene layers and large interlayer resistance.[19] Although the thermal reduction of graphene oxide films shows the promising process to produce conductive graphene films due to its low roughness level, the resistance is still high compared to the pristine graphene films. The graphene-based films prepared by exfoliation and thermal reduction process are far below the requirement for replacing ITO.

1.2 Outline

This dissertation is primarily focused on the development of a novel synthetic method and its application. Chapter 1 introduces the graphene and its fundamental concept to understand why graphene is an important and fascinating material. Chapter 2 includes an overview of the synthetic methods to produce graphene with high quality in a scalable way. The experimental section begins in Chapter 3 where we design our aqueous

arc discharge process to produce the controllable graphene layers. An experimental study of graphene application begins in Chapter 4 where we fabricate the graphene-based transparent electrodes with high transmittance. A version of Chapter 3 and 4 is submitted to *Nano Letters*. Chapter 5 reports on the graphene-based membrane for water desalination for high water permeation with high salt rejection rate. A modified form of this chapter is in preparation for submission. Chapter 6 demonstrates the novelty of an aqueous arc discharge process for multi-dimensional morphological transition strategy through the use of an oil-in-water (O/W) emulsion system. A version of this chapter is published online to *Small* (2015).

1.3 References

1. Novoselov, K. S., Geim, A. K., Morozov, S. V., Jiang, D., Zhang, Y., Dubonos, S. V., Grigorieva, I. V., Firsov, A. A. *Electric field effect in atomically thin carbon films*. Science, 2004, **306**: p. 667-669.
2. Novoselov, K. S., Geim, A. K., Morozov, S. V., Jiang, D., Katsnelson, M. I., Grigorieva, I. V., Dubonos, S. V., Firsov, A. A. *Two-dimensional gas of massless dirac fermions in graphene*. Nature, 2005, **438**: p. 197-200.
3. Zhang, Y., Tan, J. W., Stormer, H. L. Kim, P. *Experimental observation of the quantum hall effect and berry's phase in graphene*. Nature, **438**: p. 201-204.
4. Park, S., Ruoff, R. S. *Chemical methods for the production of graphene*. Nature Nanotechnol. 2009, **4**: p. 217-224.
5. Zhu, Y., Murali, S., Li, X., Suk, J. W., Potts, J. R., Ruoff, R. S. *Graphene and graphene oxide: Synthesis, properties, and applications*. Adv. Mater. 2010, **22**: p. 3906-3924.
6. Stankovich, S., Dikin, D. A., Dommett, G. H. B., Kohlhaas, K. M., Zimney, E. J., Stach, E. A., Piner, R. D., Nguyen, S. T., Ruoff, R. S. *Graphene-based composite materials.* Nature, 2006, **442**: p. 282-286.
7. Geim, A. K., Novoselov, K. S. *The rise of graphene.* Nat. Mater. 2007, **6**: p. 183-191.

8. Morozov, S. V., Novoselov, K. S., Katsnelson, M. I., Schedin. F., Elias, D. C., Jaszozak, J. A., Geim, A. K. *Giant intrinsic carrier mobilities in graphene and its bilayer.* Phys. Rev. Lett. 2008, **100**: p. 016602-016605.

9. Faccio, R., Denis, P. A., Pardo, H., Goyenola, C., Mombru, A. W. *Mechanical properties of graphene nanoribbons.* J. Phys.: Condens. Matter. 2009, **21**: p. 285304-285310.

10. Chae, H. K., Siberio-Perez, D. Y., Kim, J., Go, Y., Eddaoudi, M., Matzger, A. J., O'Keeffe, M., Yaghi, O. M. *A route to high surface area, porosity and inclusion of large molecules in crystals.* Nature, 2004, **427**: p. 523-527.

11. Stoller, M. D., Park, S. J., Zhu, Y. W., An, J. H., Ruoff, R. S. *Graphene-based ultracapacitors.* Nano Lett. 2008, **8**: p.3498-3502.

12. Scheuermann, G. M., Rumi, L., Steurer, P., Bannwarth, W., Mülhaupt, R. *Palladium nanoparticles on graphite oxide and its functionalized graphene derivatives as highly active catalysts for the Suzuki-Miyaura coupling reaction.* J. Am. Chem. Soc. 2009, **131**: p. 8262-8270.

13. Yang, W. R., Ratinac, K. R., Ringer, S. P., Thordarson, p., Gooding, J. J., Braet, F. *Carbon nanomaterials in biosensors: should you use nanotubes or graphene?* Angew. Chem. Int. Ed., 2010, **49**: p. 2114-2138.

14. Avouris, P., Chen, Z. H., Perebeinos, V. *Carbon-based electronics.* Nature Nanotechnol. 2007, **2**: p. 605-615.

15. Müllen, K., Rabe, J. P., *Nanographenes as active components of single-molecule electronics and how a scanning tunneling microscope puts them to work.* Acc. Chem. Res., 2008, **41**: p. 511-520.

16. Eda, G., Chhowalla, M. *Graphene-based composite thin films for electronics.* Nano Lett., 2009, **9**: p. 814-818.

17. Nair, R. R., Blake, P., Grigorenko, A. N., Novoselov, K. S., Booth, T. J., Stauber, T., Peres, N. M. R., Geim, A. K. *Fine structure constant defines visual transparency of graphene. Science,* 2008, **302**: p. 1308-.

18. Blake, P., Brimicombe, P. D., Nair, R. R., Booth, T. J., Jiang, D., Schedin, F., Ponomarenko, L. A., Morozov, S. V., Gleeson, H. F., Hill, E. W., Geim, A. K., Novoselov, K. S. *Graphene-based liquid crystal device.* Nano Lett. 2008, **8**: p. 1704-1708.

19. De, S., King, P. J., Lotya, M., O'Neill, A., Doherty, E. M., Hernandez, Y., Duesberg, G. S., Coleman, J. N. *Flexible, transparent, conducting films of randomly stacked graphene from surfactant-stabilized, oxide-free graphene dispersions.* Small 2010, **6**: p, 458-464.

Chapter 2. Preparation methods of graphene

2.1 Introduction

The pristine graphene has been produced by either the assembly of carbon-rich molecules such as chemical vapor deposition (CVD) and epitaxial process from silicon carbide (SiC) or mechanical exfoliation from highly ordered pyrolytic graphite (HOPG). [1-3] However, the majority of graphene research has been focused on the exfoliation and reduction process of graphite oxide due to the ease of production process. Now, the solvent-based exfoliation process has been developed to produce the pristine graphene.[4] Therefore, in this chapter, towards the mass production of graphene, the synthetic methods focus on the solvent-based exfoliation process, including the liquid phase exfoliation, graphite oxide preparation and intercalation-assisted exfoliation process.

2.2 Liquid phase exfoliation

As an efficient and low-cost method, the exfoliation of graphite in organic solvents by ultrasonication has been found to produce high quality graphene with less oxygen contents as shown in **Figure 2.1**. The liquid-phase exfoliation process basically includes three steps: (1) graphite dispersion in a solvent, (2) sonication-driven exfoliation, and (3) purification.Graphene flakes can be produced in organic solvents with surface tension around 40 mJ/m^2 followed by ultrasonication.[5] During ultrasonication, the pressure fluctuation is induced by shear forces and cavitation to the bulk graphite and leads to the exfoliation.

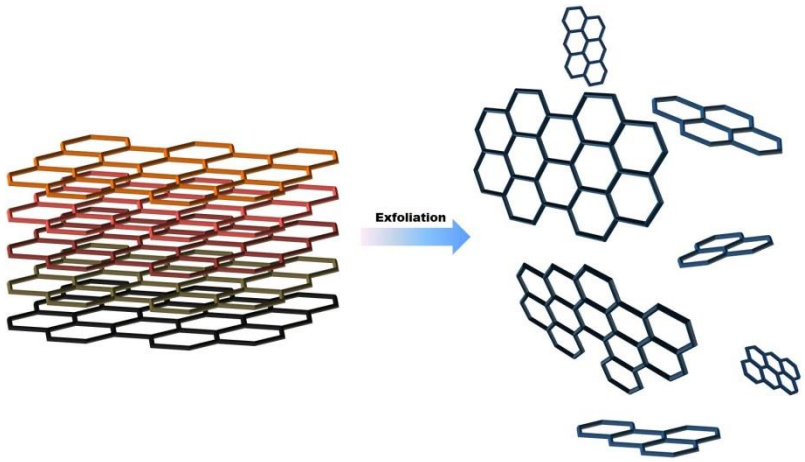

Figure 2.1 Schematic illustration of the exfoliation of graphite into graphene sheets by ultrasonication.

2.2.1 Solvent

The van der Waals (vdW) attractions between adjacent graphene are strong enough to stack each graphene layer in parallel in the interlayer distance of 3.35 Å, which makes the complete exfoliation of graphite into individual graphene layers challenging.[6] For successful exfoliation, it is required to overcome the vdWs attractions between graphene layers. In the presence of a solvent, the potential energy between adjacent graphene layers is significantly reduced compared to vacuum, which results in the reduction of the strength of the vdW attractions.[7] The interfacial tension plays an important role in the dispersion of a solid in a liquid medium. If the interfacial tension between solid and liquid is high, there is poor solubility of the solid in the liquid. In the case of graphene exfoliation in solvent, if the interfacial tension is high, the graphene flakes tend to bind together and the dispersion is very low due to its high cohesive energy to adhere to each graphene layers.[6] Solvents with surface tension, γ ~40 mJ/m^2, are the best solvents for

the dispersion of graphitic nanostructures due to its minimization of the interfacial tension between solvent and graphitic flakes as demonstrated in **Figure 2.2.**[5] However, the organic solvents used for exfoliation have drawbacks such as their high boiling point which is obstacles for the further process and toxicity for organs.[8,9]

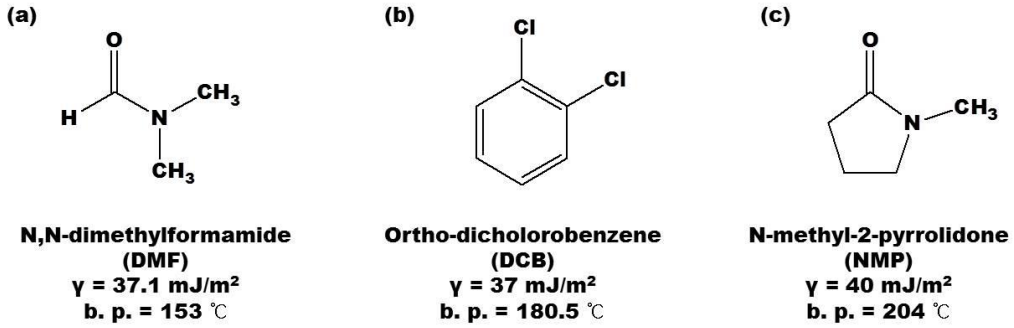

Figure 2.2 Chemical structure of common solvents used for the graphite exfoliation process.

Alternatively, a solvothermal-asisted exfoliation of expanded graphite in a highly polar organic solvent has been proposed by inducing the dipole-dipole interaction between graphene and acetonitrile, which can produce 10 wt% graphene in solution. In addition, the solvent exchange method has also been reported by exfoliating graphite in NMP and transfer the graphene flakes into ethanol, which results in 0.04 mg/mL containing 0.3 vol% NMP. [10]

2.2.2 Sonication time

Ultrasonication is an effective way to exfoliate graphene from graphite in an organic solvent due to shear force and cavitation leading to the pressure fluctuation. The longer sonication time increase in concentration of graphene up to 2 mg/mL for 500

hours. However, the increasing sonication time results in the reduced size of the graphene flakes. However, the sonication of graphite is regarded as a nondestructive process and the basal plane of the graphene is relatively defect-free, [11] it can induce to break the conjugation of graphene, which predominantly located at the edges and can affect the electronic properties of graphene.[12,13]

2.2.3 Characterization methods

The yield of liquid-phase exfoliation can be characterized providing both qualitative and quantitative information. The ideal characterization should be fast and non-destructive, give high resolution, and provide structural and electronic information. The single layer of graphene percentage is given as the ratio between the number of single layer of graphene and the total number of graphene flakes in the dispersion.[4] The concentration of the exfoliated graphene can be estimated through optical absorption spectroscopy by using the Beer-Lambert Law: $A = \alpha c l$, where A is the absorbance at 660 nm, l is the length of the optical path, and α is the absorption coefficient. α can be experimentally determined by filtering a known volume of dispersion as the dimension of [L g^{-1} m^{-1}].[4,5] The resulting concentration of the dispersion does not give information on the amount of the exfoliated graphene according to the number of stacked layers. The number of graphene layers is determined by transmission electron microscopy (TEM) and atomic force microscopy (AFM). In TEM, the number of graphene layers can be counted by visualizing the edges of the graphene flakes and by using electron diffraction patterns.[14] AFM makes the estimation of the number of graphene layers by measuring

the height of the stacked flakes and dividing them by the graphite interlayer distance.The degree of graphitization of the exfoliated graphene can be determined by Raman spectroscopy to give the degree of defects and the number of graphene layers.[15, 16]

2.3 Surfactant assisted exfoliation

The exfoliation of graphene in water is demanding due to its hydrophobic nature, which can be overcome by using surfactants. In particular, polycyclic aromatic hydrocarbons show potentials due to their π-π stacking interactions with graphene basal plane.[11]

Pyrene derivatives have been used to stabilize carbon nanotubes and graphene dispersions, which are demonstrated in **Figure 2.3.**[17] These chemical compounds can be absorbed onto the graphene surface through π-π interactions, in which they share the electrons of π-orbitals through a non-covalent bond, causing reduction of the surface free energy of the dispersion.[18] 1-pyrenesulfonic acid sodium salt was found to be the most effective pyrene derivatives to produce the high concentration of the exfoliated graphene (0.8 – 1 mg/mL), which is composed of single- or few-layered graphene.[19] The dispersion of graphene with pyrene derivatives indicates that the molecular dipole is not important, but since it facilitates adsorption on graphene, it promotes lateral displacement of water molecules collocated between the aromatic cores of the organic dye and graphene.[20] In addition, the effect of surface charges present corresponding to –OH groups has been investigated with the respective dyes at different pH.

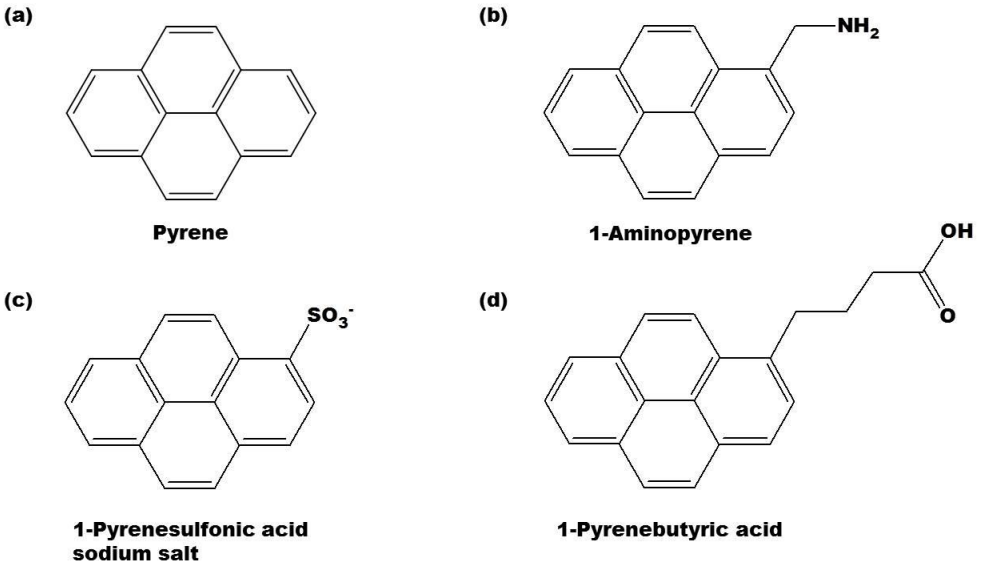

Figure 2.3 Chemical structure of pyrene derivatives used as surfactants in the process of the liquid phase exfoliation.

The exfoliation of graphene by using conventional polymers has been demonstrated in water and organic solvents. The theoretical studies have predicted that the maximum concentration of the exfoliated graphene can be obtained when the Hildebrand solubility parameters are similar between polymer, solvents and the graphene sheets.[21] However, the resulting concentration is often too low in a scalable way to produce graphene.[22] The development of polymer-solvent combination is, thus, important to produce high quality graphene dispersion at high concentrations in conventional low-polarity, low-boiling point organic solvents.[23]

A variety of ionic and non-ionic surfactants were investigated by testing the sonication-based exfoliation and dispersion of the exfoliated graphene in water shown in

Figure 2.4. Generally, the non-ionic surfactants significantly outperformed and the best result of a dispersion of graphene was achieved with a concentration of 1 mg/ml for only 2 hours sonication by using the triblock copolymer Pluronic P-123.[24] Interestingly, the yielded concentration was increased with the sonication time to 5 hours (1.5 mg/ml in P-123). Non-ionic surfactants composed of hydrophobic tail and a long hydrophilic part stabilize the graphene by steric repulsion. However, in the case of ionic surfactant, it adsorbs onto the graphene and imparts an effective charge to give electrostatic repulsion to prevent the graphene from aggregation.[25]

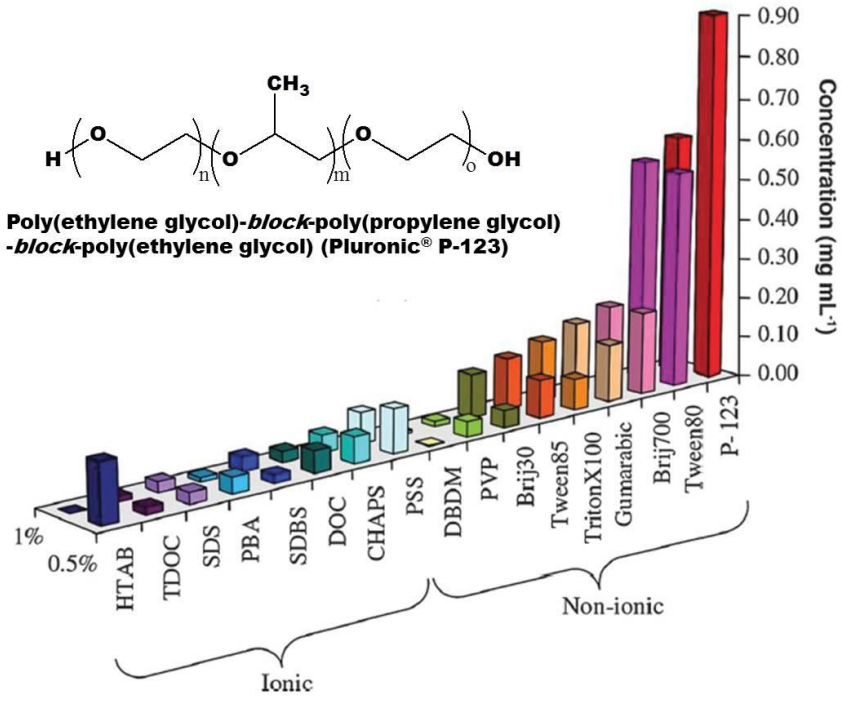

Figure 2.4 Concentration of the exfoliated graphene in aqueous solution with different surfactants. The chemical structure of non-ionic triblock copolymer P-123 is shown and the resulting concentration shows the highest concentration in a P-123 aqueous solution.

2.4 Graphene oxide preparation

Earlier attempts to isolate graphene concentrated on chemical oxidation and sonication-based exfoliation in scalable process. As a cost-effective mass production of graphene, graphene oxide (GO) is to be produced as a graphene precursor by oxidizing graphite with strong acids followed by exfoliating, which are thermally or chemically reduced into graphene.[26] The disadvantage of using graphene oxide is that the residual oxygen atoms on graphene behave as electron traps even after the reduction process. However, the low cost and easy solution process lead to a great number of investigations on enhancement of the electronic properties such as the preparation of large-sized GO sheets, chemical doping and defect repairing. [26, 27]

The preparation of large-sized GO sheets is interesting because the in-plane conductivity of basal plane of rGO is much higher than that in the vertical direction due to the large resistance in the junction between rGO sheets. [28] In order to produce the ultra-large monolayer of graphene sheets, the exfoliation of graphene oxide can occur shaking instead of the sonication process followed by centrifugation at different centrifugation speeds.[7] In addition, freeze-drying has been proven to be an efficient technique to dry GO dispersions, which facilitates the re-dispersion process.[6] Freeze-drying can keep GO sheets separated from interlayer sheets due to incorporation of a significant number of water molecules between GO sheets.[29] The absence of the sonication process of the dried GO powder is undoubtedly favorable to maintain the size of the initially produced sheets.

2.5 Conclusion

Towards the mass production of graphene, it is necessary to consider the cost-effective way with high quality. Liquid phase exfoliation methods are suitable for the mass production from the graphite oxide or graphite powders by intercalating small molecules into graphene's interlayers by increasing the interlayer distances. However, large molecules could be inserted between atomic planes, providing greater separation. In addition, the oxidation of graphite to increase the interlayer distance has also been investigated to isolate or produce graphene layers. In order to enhance the properties of graphene, the liquid phase exfoliation process should be further progressed to produce large-sized graphene/graphene oxide and increase the electrical properties.

Chapter 2 is prepared by referring the published papers in order to summarize the synthetic methods to produce high quality graphene in a scalable way.

2.6 References

1. Novoselov, K. S., Geim, A. K., Morozov, S. V., Jiang, D., Zhang, Y., Dubonos, S. V., Grigorieva, I. V., Firsov, A. A. *Electric field effect in atomically thin carbon films*. Science, 2004, **306**: p. 667-669.

2. Kim, K. S., Zhao, Y., Jang, H., Lee, S. Y., Kim, J. M., Kim, K. S., Ahn, J.-H., Kim, P., Choi, J.- Y., Hong, B. H. *Large-scale pattern growth of graphene films for stretchable transparent electrodes.* Nature 2009, **457**: p. 706–710.

3. Berger, C., Song, Z., Li, T., Li, X., Ogbazghi, A. Y., Feng, R., Dai, Z., Marchenkov, A. N., Conrad, E. H., First, P. N., and de Heer, W. A. *Ultrathin epitaxial graphite: 2D electron gas properties and a route toward graphene-based nanoelectronics.* J.

Phys. Chem. B, 2004, **108**: p. 19912-19916.

4. Shih, C. –J., Vijayaraghavan, A., Krishnan, R., Sharma, R., Han, J. –H., Ham, M. –H., Jin, Z., Lin, S., Paulus, G. L. C., Reuel, N. F., Wang, Q. H., Blankschtein, D., Strano, M. S. *Bi- and trilayer graphene solutions.* Nature Nanotechnol. 2011, **6**: p. 439-445.

5. Hernandez, Y., Nicolosi, V., Lotya, M., Blighe, F. M., Sun, Z., De, S., McGovern, I. T., Holland, B., Byrne, M., Gun'Ko, Y. K., Boland, J. J., Niraj, P., Duesberg, G., Krishnamurthy, S., Goodhue, R., Hutchison, J., Scardaci, V., Ferrari, A. C., Coleman, J. N. *High-yield production of graphene by liquid-phase exfoliation of graphite*, Nature Nanotechnol. 2008, **3**: p. 563–568.

6. Israelachvili, J. N. *Intermolecular and surface forces*, Academic press, revised 3rd ed. 2011.

7. Ciesielski, A., Samori, P. *Graphene via sonication assisted liquid-phase exfoliation.* Chem. Soc. Rev. 2014, **43**: p. 381-398.

8. Solomon, H. M., Burgess, B. A., Kennedy, G. L., Staples, R. E., *1-methyl-2-pyrrolidone (NMP): reproductive and developmental toxicity study by inhalation in the rat.* Drug Chem. Toxicol. 1995, **18**: p. 271–293.

9. Kennedy, G. L., Sherman, H. *Acute and subchronic toxicity of dimethylformam ide and dimethylacetamide following various routes of administration.* Drug Chem. Toxicol. 1986, **9**: p. 147–170.

10. Zhang, X. Y., Coleman, A. C., Katsonis, N., Browne, W. R., van Wees, B. J., Feringa, B. L. *Dispersion of graphene in ethanol using a simple solvent exchange method.* Chem. Commun. 2010, **46**: p. 7539–7541.

11. Lotya, M., Hernandez, Y., King, P. J., Smith, R. J., Nicolosi, V., Karlsson, L. S., Blighe, F. M., De, S., Wang, Z. M., McGovern, I. T., Duesberg, G. S., Coleman, J. N. *Liquid phase production of graphene by exfoliation of graphite in surfactant/water solutions.* J. Am. Chem. Soc. 2009, **131**: p. 3611–3620.

12. Park, S., An, J. H., Jung, I. W., Piner, R. D., An, S. J., Li, X. S., Velamakanni, A., Ruoff, R. S. *Colloidal suspensions of highly reduced graphene oxide in a wide variety of organic solvents.* Nano Lett., 2009, **9**: p.1593–1597.

13. Mativetsky, J. M., Liscio, A., Treossi, E., Orgiu, E., Zanelli, A., Samorı, P., Palermo, V. *Graphene transistors via in situ voltage-induced reduction of graphene-oxide under ambient conditions.* J. Am. Chem. Soc., 2011, **133**: p. 14320–14326.

14. Ferrari, A. C., Meyer, J. C., Scardaci, V., Casiraghi, C., Lazzeri, M., Mauri, F., Piscanec, S., Jiang, D., Novoselov, K. S., Roth, S., Geim, A. K. *Raman spectrum of graphene and graphene layers.* Phys. Rev. Lett., 2006, **97**: p. 187401.

15. Ferrari, A. C., Basko, D. M. *Raman spectroscopy as a versatile toll for studying the properties of graphene.* Nature Nanotechnol. 2013, **8**: p.235–246.

16. Ferrari, A. C. *Raman spectroscopy of graphene and graphite: Disorder, electron-phonon coupling, doping and nonadiabatic effects.* Solid State Commun. 2007, **143**: p. 47–57.

17. Fujigaya, T., Nakashima, N., *Methodology for homogeneous dispersion of single-walled carbon nanotubes by physical modification.* Polym. J., 2008, **40**: p. 577–589.

18. Xu, Y. X., Bai, H., Lu, G. W., Li, C., Shi, G. *Flexible graphene films via the filtration of water-soluble noncovalent functionalized graphene sheets.* J. Am. Chem. Soc., 2008, **130**: p. 5856–5857.

19. Parviz, D., Das, S., Ahmed, H. S. T., Irin, F., Bhattacharia, S., Green, M. J. *Dispersions of non-covalently functionalized graphene with minimal stabilizer.* ACS Nano, 2012, **6**: p. 8857–8867.

20. Schlierf, A., Yang, H., Gebremedhn, E., Treossi, E., Ortolani, L., Chen, L., Minoia, A., Morandi, V., Samorı, P., Casiraghi, C., Beljonne, D., Palermo, V. *Nanoscale insight into the exfoliation mechanism of graphene with organic dyes: effect of charge, dipole and molecular structure.* Nanoscale, 2013, **5**: p. 4205–4216.

21. Li, X., Zhang, G., Bai, X., Sun, X., Wang, X., Wang, E., Dai, H. *Highly conducting graphene sheets and langmuir-blodgett films.* Nature Nanotechnol. 2008, **3**: p. 538–542.

22. May, P., Khan, U., Hughes, J. M., Coleman, J. N. *Role of solubility parameters in understanding the steric stabilization of exfoliated two-dimensional nanosheets by adsorbed polymers.* J. Phys. Chem. C, 2012, **116**: p. 11393–11400.

23. Xu, L., McGraw, J.-W., Gao, F., Grundy, M., Ye, Z., Gu, Z., Shepherd, J. L. *Production of high-concentration graphene dispersions in low-boiling-point organic solvents by liquid-phase noncovalent exfoliation of graphite with a hyperbranched polyethylene and formation of graphene/ethylene copolymer composites.* J. Phys. Chem. C, 2013, **117**: p.10730–10742.

24. Guardia, L., Fernandez-Merino, M. J., Paredes, J. I., Solis-Fernandez, P., Villar-Rodil, S., Martinez-Alonso, A., Tascon, J. M. D. *High-throughput production of pristine graphene in an aqueous dispersion assisted by non-ionic surfactants.* Carbon, 2011, **49**: p. 1653–1662.

25. Bianco, A. *Graphene: Safe or toxic? The two faces of the medal.* Angew. Chem., Int. Ed., 2013, **52**: p. 4986–4997.

26. Liang, X., Chang, A. S. P., Zhang, Y., Harteneck, B. D., Choo, H., Olynick, D. L., Cabrini, S. *Electrostatic force assisted exfoliation of prepatterned few-layer*

graphenes into device sites. Nano Lett. 2009, **9**: p. 467-472.

27. Casiraghi, C., Hartschuh, A., Qian, H., Piscanec, S., Georgi, C., Fasoli, A., Novoselov, K. S., Basko, D. M., Ferrari, A. C. *Raman spectroscopy of graphene edges.* Nano Lett. 2009, **9**: p. 1433-1441.

28. Tapaszto, L., Nemes-Incze, P., Osvath, Z., Darabont, A., Lambin, P., Biro, L. P. *Electron scattering in a multiwall carbon nanotube bend junction studied by scanning tunneling microscopy.* Phys. Rev. B 2006, **74**:p. 235422.

29. De, S., King, P. J., Lotya, M., O'Neill, A., Doherty, E. M., Hernandez, Y., Duesberg, G. S., Coleman, J. N. *Flexible, transparent, conducting films of randomly stacked graphene from surfactant-stabilized, oxide-free graphene dispersions.* Small 2010, **6**:p. 458-464.

Chapter 3: Synthesis of graphene by an aqueous arc discharge

3.1 Introduction

Controllable stacking of graphene layers (less than 10 layers) is not yet possible for production of large quantities due to the lack of an effective way to separate multilayered graphene. Although several approaches for graphene production have progressed such as chemical vapor deposition (CVD),[1-2] they are still limited because they can't be produced in a scalable and cost-effective manufacturing process, such as multi-stacked layers and low efficiency.[3] Alternatively, the liquid-based exfoliation process can produce a controllable stacked number of graphene layers from graphite through ion intercalation.[4-7] Typically, the exfoliation process should overcome the van der Waals (vdW) energy, which leads to tightly bound interplanar graphene layers and the pressure needed to suppress the vdW binding is given by,[8,9]

$$P = \frac{\partial G}{\partial l} = \frac{A_{Ham}}{6\pi l^3} \qquad (1)$$

where G is the interaction free energy per unit area between two graphene layers, A_{Ham} is the Hamaker constant, and l is the interlayer distance. According to equation (1), the pressure required to separate the graphene layers is estimated to be 2.5 MPa.[8] However, the production of monolayer graphene has a low efficiency of less than 1%.[7] Otherwise, the oxygen-related functional groups in graphene oxide cannot be fully removed even after the reduction process, which leads to the deterioration of the electrical conductivity.[4, 8, 10, 11] In our previous study, the aqueous arc discharge process was developed to produce MLGs with fewer defects (low content of oxygen-related

functional groups) by exfoliating graphite in a liquid environment.[12]

Here, in this chapter, we investigated the feasibility of the aqueous arc discharge process to produce bi- and trilayers graphene towards a scalable production process. The arc discharge process was evaluated to produce graphene on the basis of the change in temperature. The aqueous arc discharge process has three features: 1) The arc discharge process is used to exfoliate the graphite electrodes, not evaporate the carbon molecules by lowering the current from the anode to the cathode. 2) The energy produced by arc discharge process can be controllable, which leads to the production of the controllable graphene layers. 3) The water used as the dielectric medium in the arc discharge process can also be used to collect the produced graphene floating on the water surface.

3.2 Experimental Section

3.2.1 Set-up of an aqueous arc discharge single reactor

The schematic of the arc discharge in the water is illustrated in Figure 2.1. High purity graphite electrodes used as anode (6 mm in diameter, 99.999%, Aldrich) and cathode (12 mm in diameter, 99.999%, Aldrich) are vertically aligned, which are submerged in deionized water (18.2 MΩ). Tow electrodes are connected to a DC power supply (Instek, SPS-3610). The anode moves up and down at 2 pps (pulses per second) to contact the fixed cathode followed by applying the voltage (25 V) to initiate arc discharge. Currents are controlled less than 4 A. Once the graphene layers are produced by the arc discharge in water, the graphene platelets migrate towards the water surface and laterally

assembled into large graphene-based films. The graphene-based films were collected by dipping the substrate or TEM grid and dried in a convection oven over night for the characterization.

3.2.2 Characterization

The morphology is observed with scanning electron microscopy (ESEM, Phillips XL30) operated at 10 kV and transmission electron microscopy (TEM, FEI Tacnai G2) with an accelerating voltage of 200 kV. X-ray photoelectron spectroscopy (XPS) measurements are performed on an AXIS Supra (Kratos) photoelectron spectrometer. C1s and O1s peaks were analyzed. Raman spectra are measured and collected using a 514 nm laser by a Reinshaw inVia Raman Microscope. The UV-vis spectra were performed using Shimadzu UV-3600 spectrometer with correction for the solvent background. Atomic force microscopy (AFM, Dimension 3100 Veeco) was performed in tapping mode with a Si tip (resonance frequency = 320 kHz; spring constant = 42 N/m). The sheet resistance was measured by Jandel four-point probe with RM 300 test.

3.3 Results and Discussion

The experimental setup for the aqueous arc discharge process to produce graphene is presented in **Figure. 3.1**. In the set-up, two graphite electrodes used as the anode and cathode were submerged in deionized water (DI water) used as a dielectric medium. The arc discharge was initiated by bringing in contact and separating the two electrodes

followed by applying a voltage (25 volts).

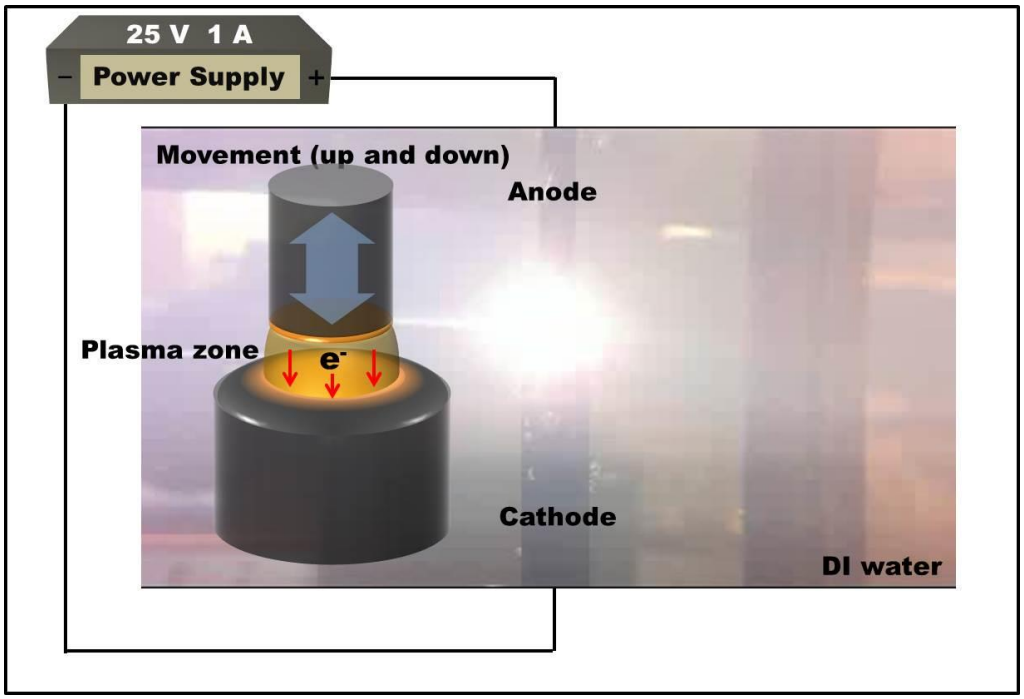

Figure 3.1 The schematic illustration of an aqueous arc discharge process. The two graphite electrodes were submerged in the water followed by applying a voltage (25 V) and current that is controllable from 1 to 4 A: the anode is moved up and down while the cathode is fixed at the bottom. The arc discharge was initiated by bringing in contact and separating the two graphite electrodes. Air bubbles emerged near the cathode due to the heating by the arc discharge.

The graphene platelets are produced from the graphite and spontaneously migrate towards the water surface followed by laterally assembling into graphene-based films on the water surface shown in **Figure 3.2**. The morphological features of the graphene-based films were investigated by scanning electron microscopy (SEM), as shown in **Figure 3.2**b. The exfoliated graphene platelets are laterally assembled with wrinkled and porous features (the white region is the substrate). Otherwise, the graphite debris falls down to the bottom and their morphology seems to be graphite powder, as shown in **Figure 3.2**c.

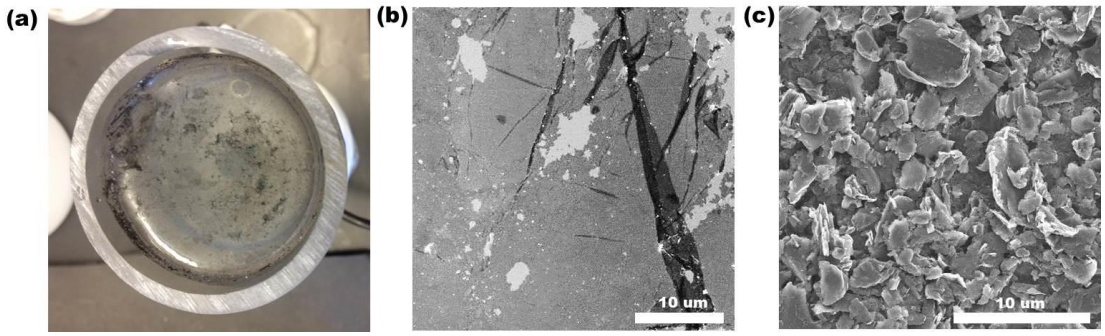

Figure 3.2 The graphene platelets. (a) A digital photo image of laterally assembled graphene platelets on the water surface. (b) Surface morphology of graphene films investigated by SEM. The laterally assembled graphene platelets were taken by dipping a Si wafer in the water surface. The white region is a Si substrate. (c) SEM image of the graphite debris falling down to the bottom of the water container during the arc discharge process.

The number of graphene layers was investigated with transmission electron microscopy (TEM), as shown in **Figure 3.3**. Bi- and tri-layer of graphene are observed in **Figure 3.3**a and b, which were produced at 1 A. The interlayer distance of graphene is presented as ~0.7 nm for three layers in **Figure 3.3**b, which means that the produced graphene in the aqueous arc discharge has the same interlayer distance with that of the pristine graphene (~0.34 nm).[13] Furthermore, the multilayered graphene (3-5 layers of graphene) are produced at a higher current level (4 A) shown in **Figure 3.3**c.

During the conventional arc discharge process in the water, the main assumptions of this process are following: (1) The reactive species such as O^+, O^{++} and H^+ ions in the plasma zone are produced by the huge amount of heat, which leads to the oxidation of carbon-based nanoparticles or the formation of CO or CO_2 gas.[14, 15] (2) The graphite electrodes evaporate and recombine carbon molecules into specific shapes of particles such as fullerene or carbon nanotubes at higher current flow (>15 A) due to rapidly

increase in temperature up to 4000 K (graphite evaporation temperature).[15-17]

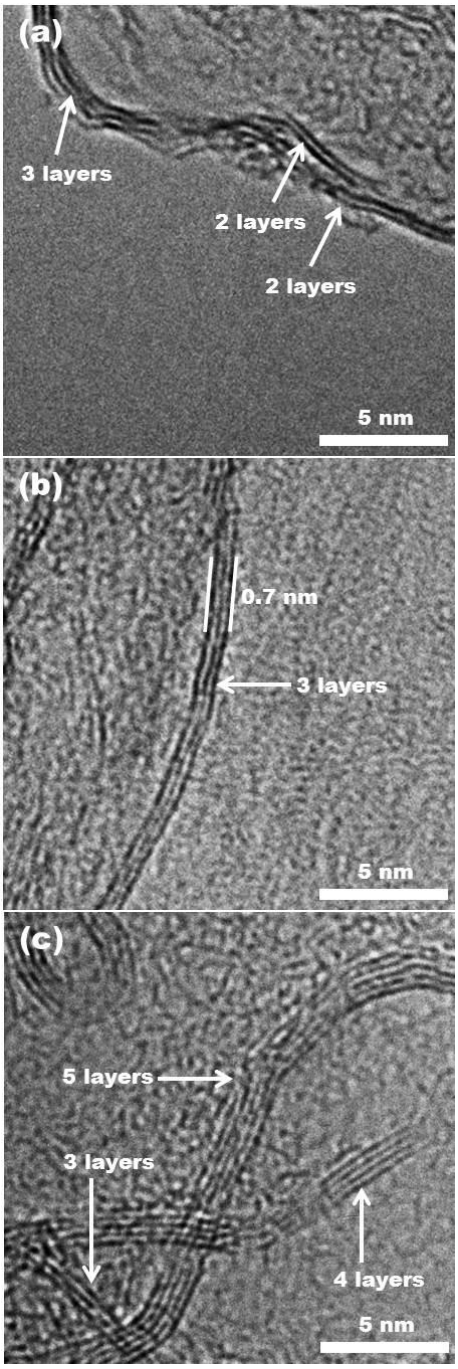

Figure 3.3 Morphological characterization of the number of stacked graphene with transmission electron microscopy (TEM). (a) Bi- and trilayers of graphene produced at 1 A. (b) Trilayers of graphene with an interlayer distance of 0.7 nm showing the same distance as that of the pristine graphene (0.35 nm). (c) Multilayered graphene sheets composed of 3 to 5 layers.

Furthermore, according to the point-heat-source model (PHSM), the electrodes erosion behavior were investigated based on the assumption that the carbon molecules are evaporated during the arc discharge process under the high current conditions.[18] However, the arc discharge process we developed uses a lower current (less than 1 amp), and the temperature is not expected to be rise up to the graphite evaporation point. The resulting temperature distribution is given by,[18]

$$T = T_0 + \frac{F_c UI}{2\pi\kappa_t r}\mathrm{erfc}\frac{r}{2\sqrt{\alpha t}} \qquad (2)$$

where T is the resulting temperature, T_0 is the ambient temperature of the graphite (298 K), F_c is the total power fraction of the cathode (0.183),[18] U is the applied voltage, I is the current, κ_t is the thermal conductivity of the graphite (2000 W m^{-1} K^{-1}), r is the size of the resulting graphene platelets, t is the pulse duration, α is the thermal diffusivity ($\alpha \equiv \rho/C_p$), C_p is the heat capacity of graphite (10.05 J mol^{-1} K^{-1}), and ρ is the graphite density (2.26 g cm^{-3}).

According to the equation (2), the resulting temperature during the arc discharge process was calculated on the basis of the size of the produced graphene platelets. For this purpose, the morphological features were investigated through atomic force microscopy (AFM) and optical microscopy. In **Figure 3.4**, the representative optical microscopic image and AFM image of the produced graphene show the planar and wrinkled 2D morphology on the substrates. In **Figure 3.4**b, the thickness of graphene sheets produced at 1 A is 1.399 nm, which indicates that the number of stacked layers of graphene is 3 based on the fact that TEM image (**Figure 3.3**) reveals that the distance between layers is 0.34 nm. Otherwise, the thickness of graphene sheets produced at 4 A is

4.8 nm, which indicates that the number of stacked graphene layers is 7 to 8 layers. The size distribution was analyzed by optical microscopy.

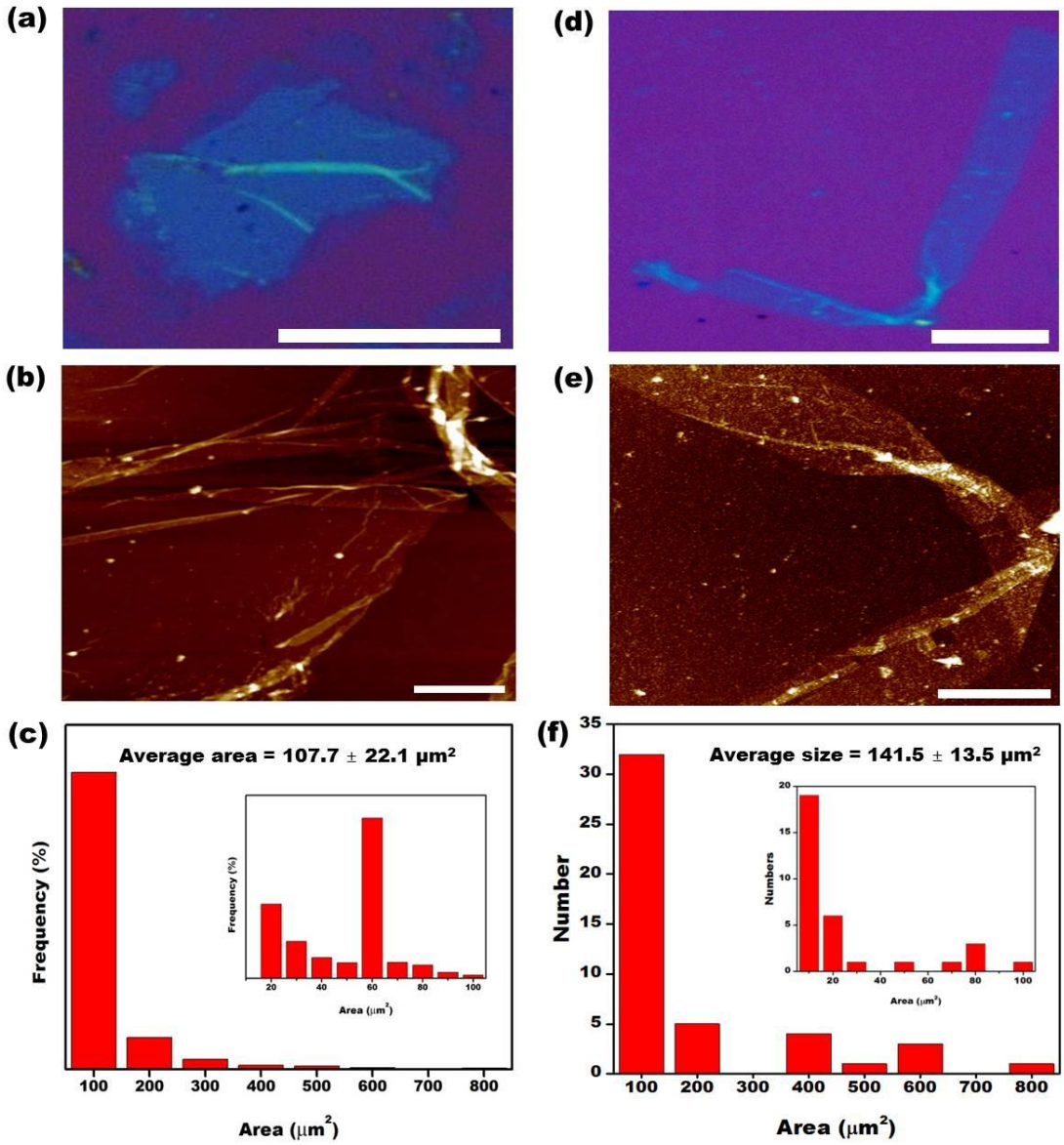

Figure 3.4 Optical characterization for the size distribution of graphene produced at 1 A and 4 A. (a) optical microscopic image and (b) atomic force microscopy (AFM) image demonstrates the morphological features of the exfoliated graphene produced at 1 A and (c) the size distribution of the exfoliated graphene produced at 1 A. (d) optical microscopic image and (e) AFM image demonstrate the morphological features. (e) the size distribution of the exfoliated graphene produced at 4 A.

Graphene sheets on SiO_2/Si substrate were observed to be 300 nm thick of SiO_2, as shown in Figure 3.4a and b. **Figure 3.4**c and d shows that the area distribution of the multi-layered graphene produced at 1 A is 107.7 ± 22.1 μm^2 and the range of the average size is 4.4 to 28.3 μm. Likewise, the size distribution of the graphene produced at 4 A is 141.5 ± 13.5 μm^2 and the range of the average size is 4.4 to 28.3 μm.

In **Figure 3.5**, the resulting temperatures were calculated based on the resulting size distribution according to equation (2) at each different current from 1 to 4 A in order to evaluate the mechanism. At lower currents (<1 A), the maximum temperature is about 703 K and the minimum temperature is about 352 K. In addition, the calculated temperature ranges are 1108 to 406 K, 1513 to 460 K, and 1919 and 514 K at 2 A, 3 A and 4 A, respectively. The temperatures are significantly lower than that of the conventional arc discharge process (>15 A), which will rise up to 4000 K to evaporate carbon molecules. This leads to the conclusion that our system is not evaporating the carbon molecules from the graphite electrodes, but thermally assisted exfoliating the graphene sheets from the graphite electrodes.

During the arc discharge in water, the surface of the graphite near the arc plasma zone is thermally expanded by rapid heating up to 703 K at 1 A followed by evaporating the water and refilling the gap between the electrodes. The produced graphene platelets move towards the water surface by water flushing through the gap in the electrodes. In the case of thermal exfoliation of graphene oxide, the graphite oxide or graphite is thermally expanded from 300 ℃ to 1050 ℃ followed by an ultrasonication process, which induces the mechanical tension by varying the pressure.[8, 9] In addition, the rapid heating through arc discharge induces the water cavitation (bursting water bubbles) and

the cavitation pressure was found to be 17 MPa at 80 ℃.[19]

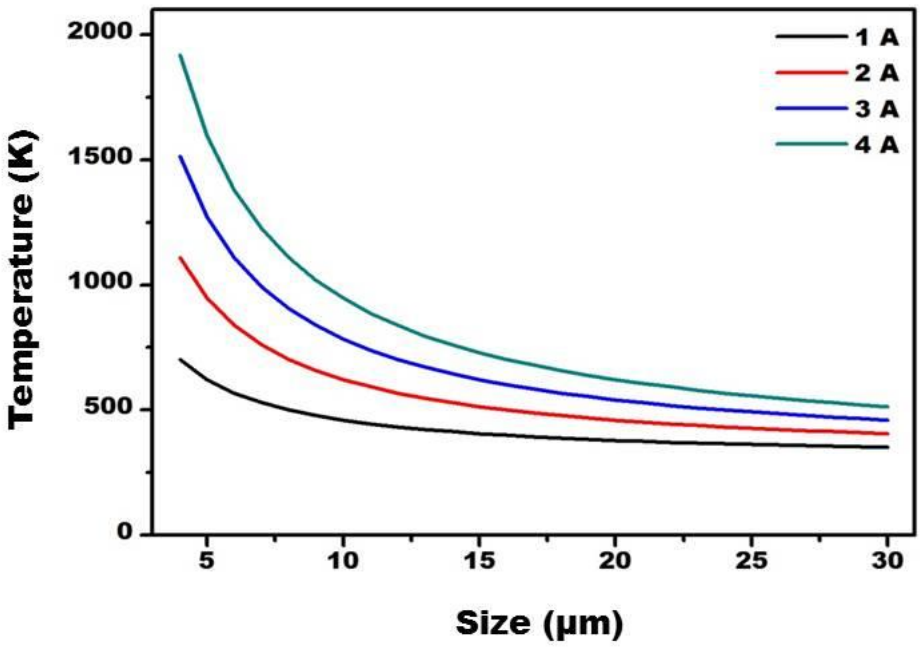

Figure 3.5 The calculated temperature during an arc discharge in water at 1, 2, 3, and 4 A, respectively. The calculated temperature will rise up to less than 2000 K, which is not enough to evaporate the carbon molecules in our arc discharge process. The graphene is produced by thermally assisted exfoliation from the graphite, not evaporation of carbon molecules.

Furthermore, the recent studies demonstrated that the minimum exfoliation energy for multi-layered graphene (MLG) is around 0.4 MPa, which demonstrates that MLGs were electrostatically exfoliated at an air by overcoming the cohesive energy between the interlayer graphene.[20] In our case, the arc discharge process induces the pressure change during the process, which is defined as the minimum stress required for fully separating a graphene monolayer from the bulk graphite. Therefore, to our system, we assumed that the mechanism producing the graphene platelets is the combination of

thermal expansion of graphite and the water cavitation through rapid heating by arc discharge.

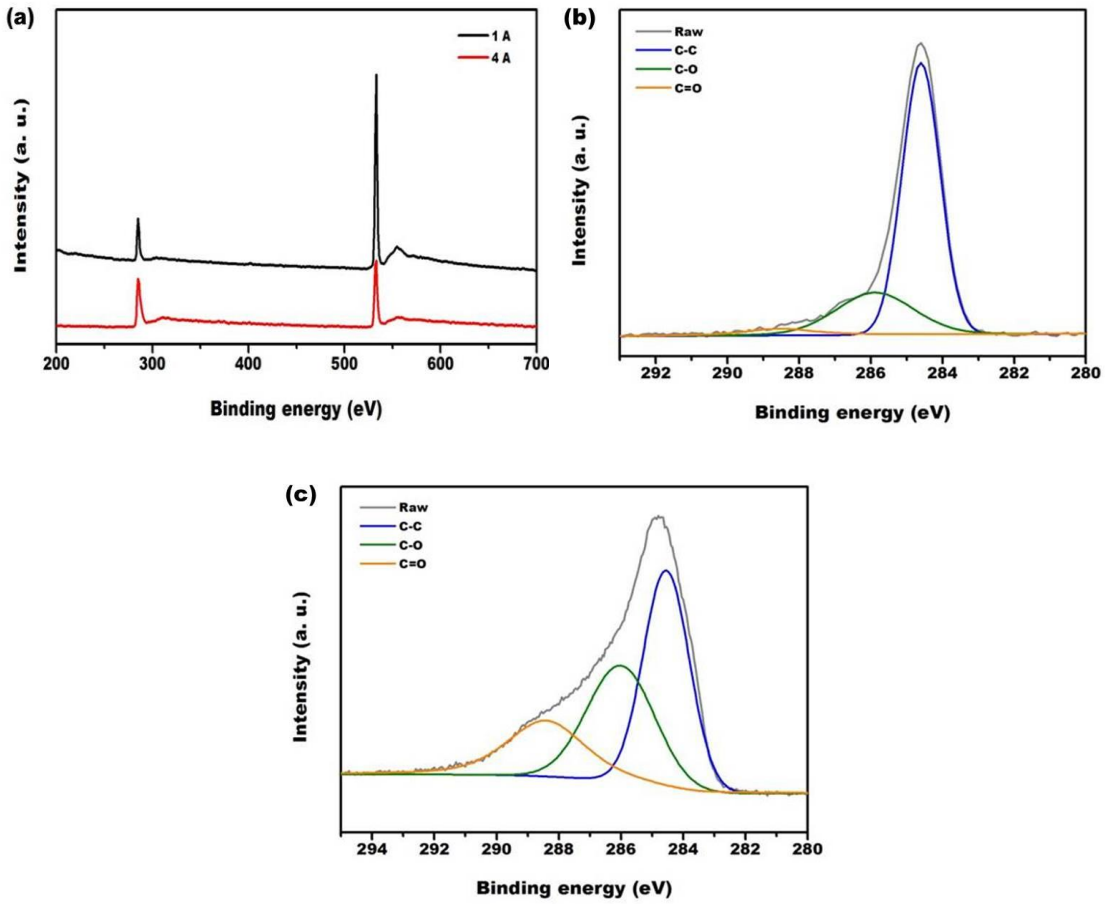

Figure 3.6 X-ray photoemission spectroscopy (XPS) characterization. (a) XPS wide scan and deconvolution of the produced graphene at currents below 1 A (black solid line) and 4 A (red solid line), respectively, showing the carbon and oxygen in the produced graphene. (b) Deconvolution of C1s for the exfoliated graphene from the current at 1 A. (c) Deconvolution of C1s for the exfoliated graphene from the current at 4 A.

The emerging gas inside the graphite/graphite oxide is needed to split the interlayers by diffusion.[8, 9] In our arc discharge process, the reactive species such as O^{+}, O^{++}, and H^{+} were produced followed by the formation of CO/CO_2 gas,[12] which might

result in the oxidation of carbon molecules in the graphene platelets. In order to validate our first assumption on the oxidation, X-ray photoelectron spectroscopy (XPS) was performed as a direct means to estimate the oxygen-related defects. These reactive species result in the oxidation of graphene while the arc discharge is in process.

Results for the XPS analysis are shown in **Figure 3.6**. In wide-scan XPS spectra in **Figure 3.6**a, the peaks appearing at 284.90 eV and 532.90 eV can be assigned to C1s and O1s, respectively, which indicate the oxidation of graphene during the arc discharge in water. High-resolution C1s XPS spectrum for graphene at currents of 1 and 4 A are shown in **Figure 3.6**b and c. Deconvolution of the spectra of graphene at 1 A indicates that the relative content of the non-oxygenated ring C atoms (284.5 eV) was 71.9%, that of C atoms in C-O bonds (285.9 eV) was 20.8%, and that of carboxylate C atoms (O-C=O, 288.15 eV) was 7.3%, shown in **Figure 3.6**b. Moreover, deconvolution of high-resolution C1s spectra of the produced graphene at 4 A indicates that the relative content of the non-oxygenated ring C atoms (284.4 eV) was 46.1%, that of C atoms in C-O bonds (286.2 eV) was 34.8%, and that of carboxylate C atoms (O-C=O, 288.5 eV) was 19.1%, shown in **Figure 3.6**c. Based on the XPS data, the defects on the graphene arise from the oxidation by reactive species in the plasma zone, and the relative content of the non-oxygenated ring C atoms is independent of the level of the current. Therefore, the chemical composition of the graphitic carbon particles produced by the arc discharge is comparable to the reduced graphene oxide sheets through the one-step process. Raman spectroscopy is an effective way to evaluate the crystalline quality of the graphitic carbon structure shown in **Figure 3.7**. The intensity of the D-peak, G-peak and 2D peak are associated with defects, graphitic structure and the number of stacked graphene layers at

1351, 1578, and 2660 cm^{-1}.[21-23] Generally, the 2D peaks indicate that the monolayer of graphene appears at 2660 cm^{-1}, and the peak shifts to 2690 cm^{-1} with an increase in the number of stacked layers.[31] In Figure 3.7b, the relative intensity ratio of I_D/I_G associated with the degree of defects is decreased with increasing current during the arc discharge: the I_D/I_G is 0.54, 0.46, 0.55 and 0.14 at 1, 2, 3 and 4 A, respectively.

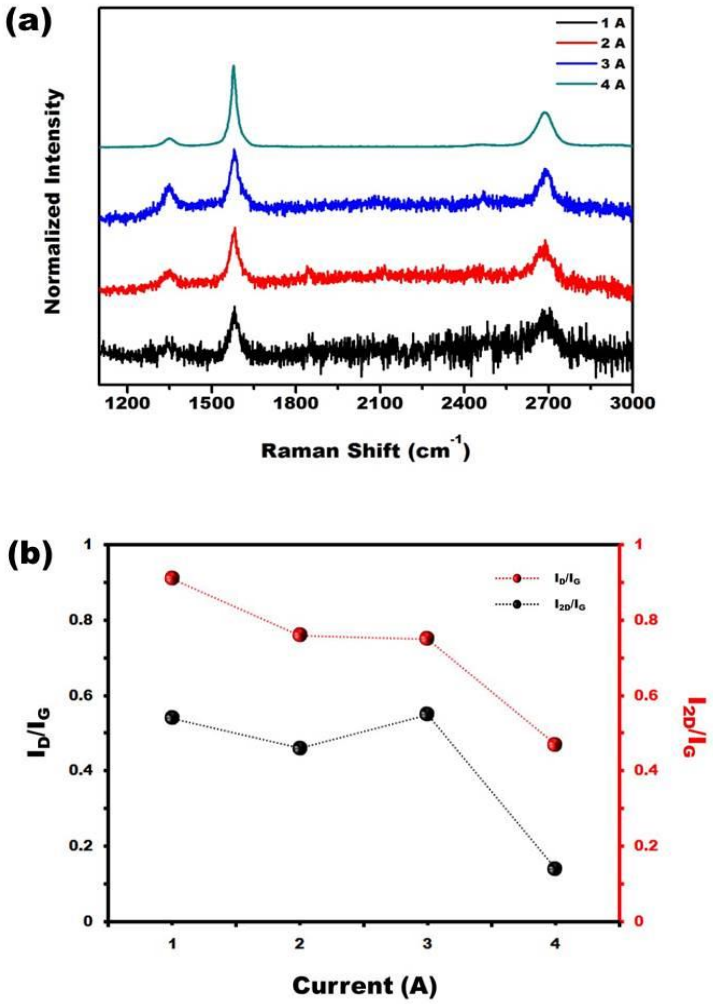

Figure 3.7 Optical characterization by Raman spectroscopy. (a) Raman spectroscopy of the exfoliated graphene at four different current level from 1 A to 4 A. (b) Relative intensity ratio of I_D/I_G (black solid line) and I_{2D}/I_G (red solid line) for the exfoliated graphene.

Furthermore, the relative intensity ratio of I_{2D}/I_G is 0.91 at 1 A, which corresponds to bi- and trilayers. Accordingly, the 2D peak at 2660 cm^{-1} at 1 A is shown and the other spectral component at 2690 cm^{-1} gradually dominates with increasing current. Interestingly, the intensity ratio of I_D/I_G is decreased from 0.54 to 0.14 with increasing current even though the oxygen content on the graphene stays at the same level as it is at the lower current condition. The degree of defects might be affected by the graphene size edge effect that the edge states characterized by high density of defects and increased doping level was demonstrated.[22, 23]

3.4 Conclusion

In summary, we have demonstrated the aqueous arc discharge process to produce bi-and trilayers of graphene in a potential scalable process. Compared to the conventional process, the produced graphene is exfoliated from the graphite electrodes through thermal expansion and water cavitation by rapid heating. In addition, the adjustable arc discharge power leads to controllable stacked numbers of graphene layers. The produced graphene layers have defects from the oxygen-related functional group and edge effects due to its small size. The exfoliated graphene has the feasibility to be used in transparent electrodes with high transmittance (>90 % at 550 cm^{-1}) and 350 $k\Omega/cm^2$ by transferring graphene films into any substrate. In the future, there is still the need to optimize the production of a monolayer of graphene by adjusting the arc discharge power and the properties of the dielectric medium in a practical scalable way. In addition, the byproduct of the multilayered graphene should be separated in a seamless process.

Chapter 3, in part, has been submitted for publication of the material as it may appear in Nano Letters: Sejung Kim, Youngjun Song, Jennifer Marciniak, and Michael J. Heller, Bi- and trilayers graphene in an aqueous arc discharge process. The dissertation author was the primary investigator and author of this material.

3.5 References

1. Li, X., Cai, W., An, J., Kim, S., Nah, J., Yang, D., Piner, R., Velamakanni, A., Jung, I., Tutuc, E., Banerjee, S. K., Colombo, L., Ruoff, R. S. *Large-area synthesis of high-quality and uniform graphene films on copper foils.* Science, 2009, **324**: p. 1312-1314.

2. Bae, S., Kim, H., Lee, Y., Xu, X., Park, J. –S., Zheng, Y., Balakrishnan, J., Lei, T., Kim, H. R., Song, Y. I., Kim, Y. –J., Kim, K. S., Ö zyilmaz, B., Ahn, J. –H., Hong, B. H., Iijima, S. *Roll-to-roll production of 30-inch graphene films for transparent electrodes.* Nat. Nanotechnol. 2010, **5**: p. 574-578.

3. Zurutuza, A., and Marinelli, C. *Challenges and opportunities in graphene commercialization.* Nat. Nanotechnol. 2014, **9**: p. 730-734.

4. Wang, H., Robinson, J. T., Li, X., Dai, H. *Solvothermal reduction of chemically exfoliated graphene sheets.* J. Am. Chem. Soc. 2009, **131**: p. 9910-9911.

5. Eigler, S., Enzelberger-Heim, M., Grimm, S., Hofmann, P., Kroener, W., Geworski, A., Dotzer, C., Röckert, M., Xiao, J., Papp, C., Kytken, O., Steinrück, H. –P., Hirsch, A. *Wet chemical synthesis of graphene.* Adv. Mater. 2013, **25**: p. 3583-3587.

6. Shih, C. -J., Vijayaraghavan, A., Krishnan, R., Sharma, R., Han, J. –H., Ham, M. –H., Jin, Z., Lin, S., Paulus, G. L. C., Reuel, N. F., Wang, Q. H., Blankschtein, D., Strano, M. S. *Bi- and trilayer graphene solutions.* Nat. Nanotechnol. 2011, **6**: p. 439-445.

7. Hernandez, Y., Nicolosi, V., Lotya, M., Blighe, F. M., Sun, Z., De, S., McGovern, I. T., Holland, B., Byrne, M., Gun'ko, Y. K., Boland, J. J., Niraj, P., Duesberg, G., Krishnamurthy, S., Goodhue, R., Hutchison, J., Scardaci, V., Ferrari, A. C., Coleman, J. N. *High-yield production of graphene by liquid-phase exfoliation of graphite.* Nat. Nanotechonol. 2008, **3**: p. 563-568.

8. McAllister, M. J., Li, J. –L., Adamson, D. H., Schniepp, H. C., Abdala, A. A., Liu,

J., Herrera-Alonso, M., Milius, D. L., Car, R., Prud'homme, R. K., Aksay, I. A. *Single sheet functionalized graphene by oxidation and thermal expansion of graphite*. Chem. Mater. 2007, **19**: p. 4396-4404.

9. Schniepp, H. C., Li, J. –L., McAllister, M. J., Sai, H., Herrera-Alonso, M., Adamson, D. H., Prud'homme, R. K., Car, R., Saville, D. A., Aksay, I. A. *Functionalized single graphene sheets derived from splitting graphite oxide.* J. Phys. Chem. B 2006, **110**: p. 8535-8539.

10. Su, C. –Y., Xu. Y., Zhang, W., Zhao, J., Tang, X., Tsai, C. –H., Li, L. –J. *Electrical and spectroscopic characterization of ultra-large reduced graphene oxide monolayers.* Chem. Mater. 2009, **21**: p. 5674-5680.

11. Cote, L. J., Kim, F., Huang, J. *Langmuir-blodgett assembly of graphite oxide single layers.* J. Am. Chem. Soc. 2009, **131**: p. 1043-1049.

12. Kim, S., Song, Y., Takahashi, T., Oh, T., Heller, M. J. *An aqueous single reactor arc discharge process for the synthesis of graphene nanospheres.* Small 2015, **11**: p. 5041-5046.

13. Girifalco, L. A., and Lad, R. A. *Energy of cohesion, compressibility, and the potential energy functions of the graphite system.* J. Chem. Phys. 1956, **25**: p. 693-697.

14. Eubank, P. T., Patel, M. R., Barrufet, M. A., Bozkurt, B. *Theoretical models of the electrical discharge machining process. III. The variable mass, cylindrical plasma model.* J. Appl. Phys. 1993, **73**: p. 7900-7909.

15. Sano, N., Wang, H., Alexandrou, I., Chhowalla, M., Teo, K. B. K., Amaratunga, G. A. J. *Properties of carbon onions produced by an arc discharge in water.* J. Appl. Phys. 2002, **92**: p. 2783-2788.

16. Sano, N., Wang, H., Chhowalla, M., Alexandrou, I., Amaratunga, G. A. J. *Synthesis of carbon 'onions' in water.* Nature 2001, **414**: p. 506-507.

17. Hsin, Y. L., Hwang, K. C., Chen, F. –R., Kai, J. –J. *Production and in-situ metal filling of carbon nanotubes in water.* Adv. Mater. 2001, **13**: p. 830-833.

18. DiBitonto, D. D., Eubank, P. T., Patel, M. R., Barrufet, M. A. *Theoretical models of the electrical discharge machining process. I. A simple cathode erosion model.* J. Appl. Phys. 1989, **66**: p. 4095-4103.

19. Herbert, E., Balibar, S., and Caupin, F. *Cavitation pressure in water.* Phys. Rev. E 2006, **74**: p. 041603.

20. Liang, X., Chang, A. S. P., Zhang, Y., Harteneck, B. D., Choo, H., Olynick, D. L., Cabrini, S. *Electrostatic force assisted exfoliation of prepatterned few-layer graphenes into device sites.* Nano Lett. 2009, **9**: p. 467-472.

21. Ferrari, A. C., Meyer, J. C., Scardaci, V., Casiraghi, C., Lazzeri, M., Mauri, F., Piscanec, S., Jiang, D., Novoselov, K. S., Roth, S., Geim, A. K. *Raman spectrum of graphene and graphene layers.* Phys. Rev. Lett. 2006, **97**: p. 187401.

22. Casiraghi, C., Hartschuh, A., Qian, H., Piscanec, S., Georgi, C., Fasoli, A., Novoselov, K. S., Basko, D. M., Ferrari, A. C. *Raman spectroscopy of graphene edges.* Nano Lett. 2009, **9**: p. 1433-1441.

23. Li, Q. –Q., Zhang, X., Han, W. –P., Lu, Y., Shi, W., Wu, J. –B., Tan, P. –H. *Raman spectroscopy at the edges of multilayer graphene.* Carbon 2015, **85**: p. 221-224.

24. Parvez, K., Li, R., Puniredd, S. R., Hernandez, Y., Hinkel, F., Wang, S., Feng, X., Mullen, K. *Electrochemically exfoliated graphene as solution-processable, highly conductive electrodes for organic electronics.* ACS Nano 2013, **7**: p. 3598-3606.

Chapter 4: Transparent electrodes

4.1 Introduction

Indium tin oxide (ITO) based transparent electrodes are a fundamental part of optoelectronic devices, and are the market standard for many applications.[1-3] In the case of thin film solar cells, ITO-based electrodes are used as the hole collecting layers with high transmittance (> 90% at a wavelength of 500 nm), low sheet resistance of 10 to 30 Ω cm^{-2} and a favorable work function of ~4.8 eV.[1-3] However, the use of ITO has limitations due to the scarcity of indium, incompatibility with acid and basic conditions, and high surface roughness.[1-3] In addition, its brittleness is a major challenge for applications in flexible electronic devices such as flexible displays, solar cells and touch screens.[4-7] Therefore, the alternative transparent electrodes have been investigated in order to replace ITO, such as metallic nanowires, conductive polymers and carbon nanotubes.[8-10] Among these perspective materials for transparent electrodes, carbon nanotubes films have been found to exhibit high transmittance for the whole visible light range. However, the limitation of using carbon nanotubes films is the difficulty of avoiding the formation of a percolation network.[11-13] The percolated junction between nanotubes limits the conductive pathway due to its high resistance. Since the first isolation of graphene, it has been shown to have outstanding physical properties such as high chemical and thermal stability, high stretchability, and low contact resistance with organic materials.[14-16] Most of all, monolayer graphene possess high crystallographic quality and ballistic electron transport with low light absorption (2.3%) making it a promising alternative to ITO electrodes.[17,18]

In this chapter, we produced multi-layered graphene with less than 10 layers by an aqueous arc discharge process we developed. We used this method to fabricate graphene-based transparent electrodes on the transparent flexible substrates. The exfoliated graphene was collected by vacuum-assisted filtration and re-dispersed into N-methyl-2-pyrrolidone (NMP) followed by deposition on a commercial nylon membrane. The graphene-based membranes were transferred onto the transparent flexible substrate and the thickness was controlled by adjusting the dispersion concentration. The transmittance and the sheet resistance were measured in order to investigate the capability to replace ITO-based transparent electrodes.

4.2 Experimental Section

4.2.1 Synthesis of graphene by an arc discharge in water

High purity graphite electrodes were used as an anode (6 mm in diameter, 99.999%, Aldrich) and a cathode (12 mm in diameter, 99.999%, Aldrich) and were vertically aligned and submerged in deionized water (18.2 MΩ). The two electrodes are connected to a DC power supply (Instek, SPS-3610). The anode moved up and down at 2 pps (pulses per second) to contact the fixed cathode followed by application of a voltage (25 V) to initiate arc discharge. The current was controlled to be less than 1 A. Once the graphene layers were produced by the arc discharge in water, the graphene platelets migrated towards the water surface and laterally assembled into large graphene-based films. The graphene-based films were collected by dipping the substrate or TEM grid into

the water and were dried in a convection oven over night for characterization.

4.2.2 Transfer graphene-based films into substrates

The exfoliated graphene was collected on a nylon membrane with a 0.45 μm pore size by vacuum filtration and washed with water several times. The collected particles were then dispersed into NMP by sonication for 5 min in order to prevent further exfoliation. The dispersed graphene solution was left to stand over-night in order to separate the multilayered graphene. The resulting graphene solution was collected again with a nylon membrane by vacuum filtration followed by drying at 85 ℃ for 2 hours. The graphene particles on the membrane were transferred into a poly(ethyleneterephthalate) (PET) by pressing. After transfer, the graphene-based films on the substrate were dried at 85 ℃ for 2 hours to remove residual solvent.

4.2.3 Characterization

The morphology of the graphene-based films was analyzed using both scanning electron microscopy (ESEM, Phillips XL30) operated at 10 kV and transmission electron microscopy (TEM, FEI Tacnai G2) with an accelerating voltage of 200 kV. X-ray photoelectron spectroscopy (XPS) measurements were performed on an AXIS Supra (Kratos) photoelectron spectrometer. C1s and O1s peaks were analyzed. Raman spectra are measured and collected using a 514 nm laser by a Reinshaw inVia Raman Microscope.

The UV-vis spectra was performed using Shimadzu UV-3600 spectrometer and was corrected for the solvent background. Atomic force microscopy (AFM, Dimension 3100 Veeco) was performed in tapping mode with a Si tip (resonance frequency = 320 kHz; spring constant = 42 N/m). The sheet resistance was measured by a Jandel four-point probe with RM 300 test.

4.3 Results and Discussion

The aqueous arc discharge process we developed involved two graphite electrodes used as the anode and cathode which were submerged in a dielectric deionized water medium. The arc discharge was initiated by repeatedly bringing the two electrodes into contact and then separating them while applying a voltage (25 V, ~1 A). The graphene platelets were produced from the graphite and the number of graphene layers was determined using transmission electron microscopy (TEM), as shown in **Figure 4.1**. Three- and six-layers of graphene were observed which were produced at 1 A. The interlayer distance of graphene was measured at ~0.7 nm for three layers in **Figure 4.1**a, which means that the graphene produced in the aqueous arc discharge has the same interlayer distance as the pristine graphene (~0.34 nm).[19]

In **Figure 4.2**, the representative AFM image of the produced graphene shows the planar and wrinkled 2D morphology on the substrates, which are a common feature of graphene. The thickness of the graphene sheets is 1.399 nm, which indicates that there are ~3 stacked layers of graphene based on the ~0.34 nm distance between layers as shown in **Figure 4.1**. In **Figure 4.2**b, the graphene platelets produced at 1 A are largely composed

of bi- and trilayers of graphene (73%) and multilayered graphene. In order to compare the number of layers at different current levels, four to seven layered graphene (78%) was produced at 4 A.

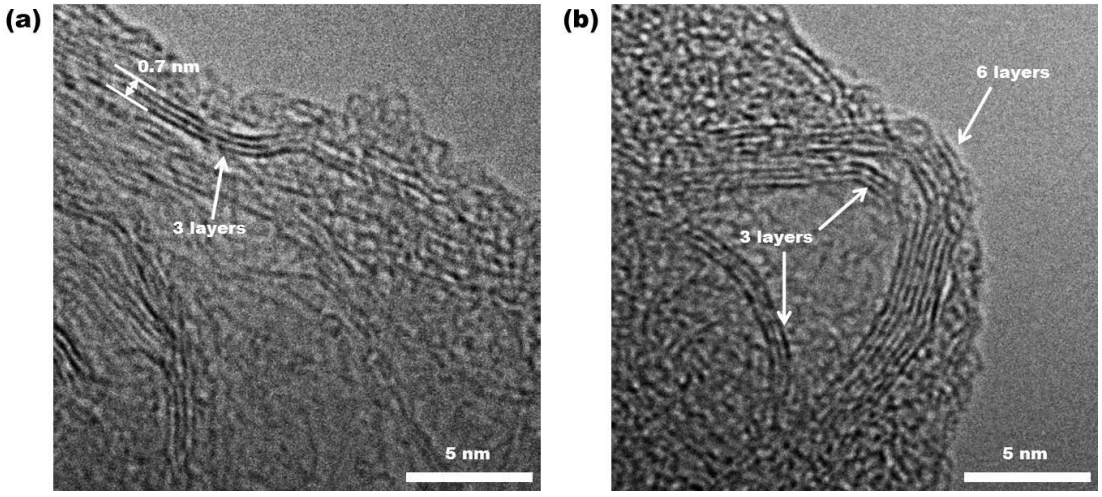

Figure 4.1 TEM images of the exfoliated graphene. (a) Three layers of graphene with an interlayer distance of 0.7 nm. (b) three and six-layers of graphene. The exfoliated graphene was produced with less than 1 A during the arc discharge process.

In **Figure 4.2**, the representative AFM image of the produced graphene shows the planar and wrinkled 2D morphology on the substrates, which are a common feature of graphene. The thickness of the graphene sheets is 1.399 nm, which indicates that there are ~3 stacked layers of graphene based on the ~0.34 nm distance between layers as shown in **Figure 4.1**. In **Figure 4.2**b, the graphene platelets produced at 1 A are largely composed of bi- and trilayers of graphene (73%) and multilayered graphene. In order to compare the number of layers at different current levels, four to seven layered graphene (78%) was produced at 4 A.

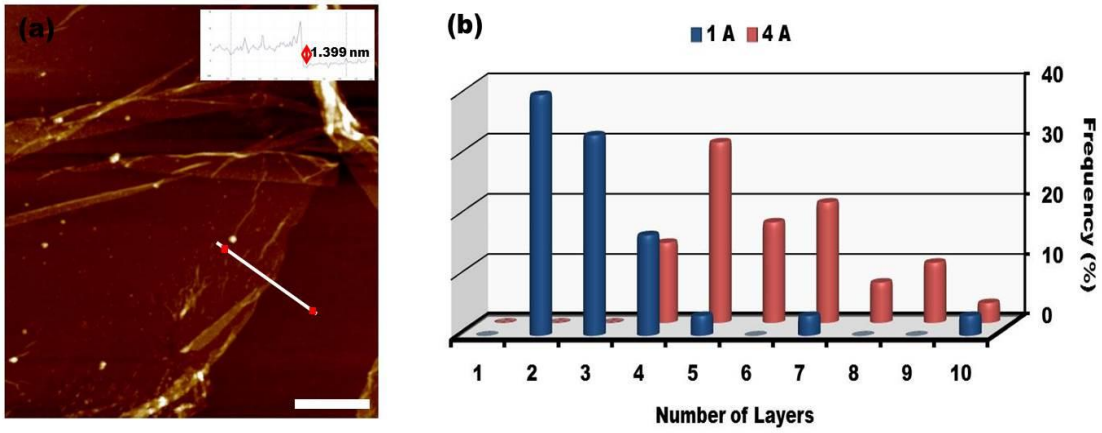

Figure 4.2 The distribution of the number of graphene layers. (a) a representative AFM image of the exfoliated graphene with wrinkled and planar surface with a height of 1.399 nm. (b) the distribution of the number of graphene layers.

In order to find the concentration of the graphene sheets, the exfoliated graphene dispersion in NMP was filtered through a polyvinylidene fluoride (PVDF) membrane. The measurement of the filtered mass gave the concentration of the exfoliated graphene in NMP. The dispersions were then characterized by UV-vis spectrometer to measure the absorbance corresponding to the different concentrations. The absorption is shown in **Figure 4.3**, were the concentration was calculated by measuring the filtered mass. According to the absorbance at 660 nm, which was divided by cell length, and is plotted versus dispersion concentration (**Figure 4.3**b), Lambert-Beer behavior is observed and the absorption coefficient, α, is 2744 L g^{-1} cm^{-1}.

To explore the utility of our high-quality graphene, we fabricated graphene-based transparent electrodes on poly(ethylene terephthalate) (PET) films using a vacuum filtration and dry pressing transfer method.[20] As the schematic process demonstrates in **Figure 4.4**, the exfoliated graphene dispersion in *N*-methyl-2-pyrrolidone (NMP) was

first collected on a nylon membrane by vacuum filtration. The filtered graphene-based film was dried overnight followed by pressing onto a transparent PET substrate overnight at 35 ℃. Once the nylon membrane was peeled away, the graphene-based film remained on a PET substrate due to van der Waals (vdW) interactions between the graphene and the PET substrate.

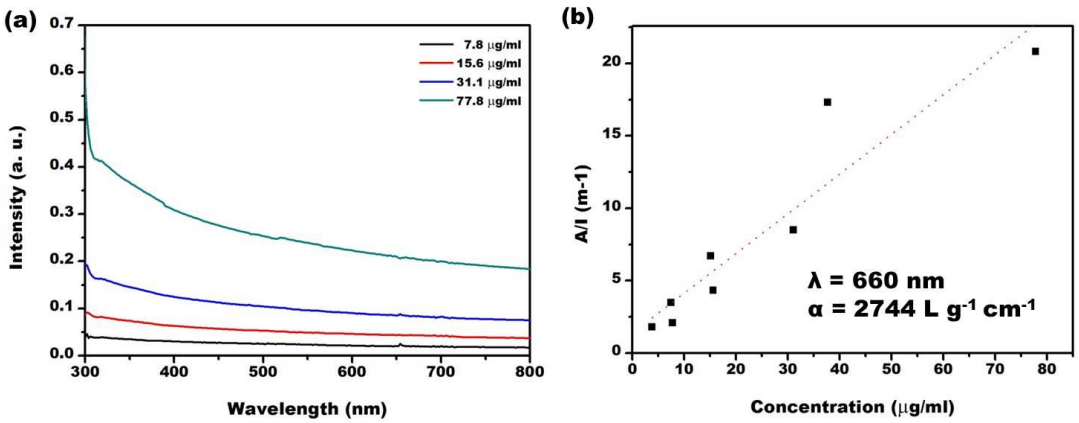

Figure 4.3 The concentration of the exfoliated graphene in NMP. (a) The absorbance of the exfoliated graphene in NMP according to different concentrations from 7.8 μg/ml to 77.8 μg/ml. (b) The Lambert-Beer behavior and the absorption coefficient at a wavelength of 660 nm, $<\alpha_{660nm}> = 2744$ L g^{-1} cm^{-1}.

To explore the utility of our high-quality graphene, we fabricated graphene-based transparent electrodes on poly(ethylene terephthalate) (PET) films using a vacuum filtration and dry pressing transfer method.[20] As the schematic process demonstrates in **Figure 4.4**, the exfoliated graphene dispersion in *N*-methyl-2-pyrrolidone (NMP) was first collected on a nylon membrane by vacuum filtration. The filtered graphene-based film was dried overnight followed by pressing onto a transparent PET substrate overnight at 35 ℃. Once the nylon membrane was peeled away, the graphene-based film remained

on a PET substrate due to van der Waals (vdW) interactions between the graphene and the PET substrate. **Figure 4.5** shows the resulting graphene-based membrane and the surface of the nylon filter after peel-off. The representative thickness of vacuum-assisted graphene films is 50 nm, shown in **Figure 4.5**a, and the thickness was controlled by the concentration of graphene dispersion in NMP according to the relationship between the intensity of the UV-vis spectrum and concentration, as shown in **Figure 4.3**a. Once the graphene-based membranes were peeled off, the residual graphene flakes were randomly distributed on the nylon filters and were not observed to be interconnected.

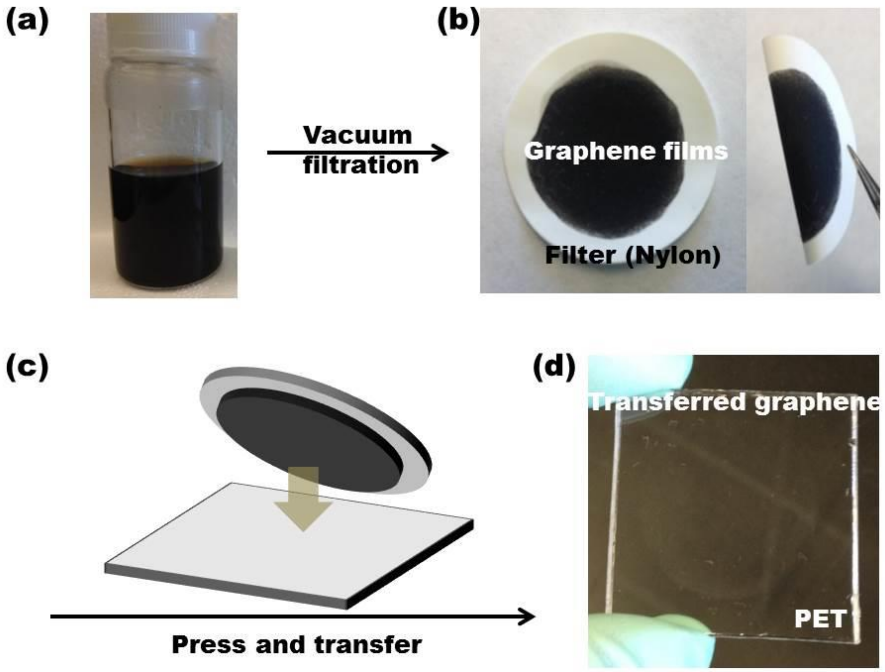

Figure 4.4 Drying transfer process. (a) The dispersion of the exfoliated graphene in NMP was filtered by vacuum filtration. (b) The resulting graphene-based membranes on nylon filter were dried at 35 ℃ overnight. (c) The graphene-based film on nylon filter was transferred onto the poly(ethylene terephthalate) (PET) film. (d) The resulting transferred graphene-based films on a transparent PET substrate.

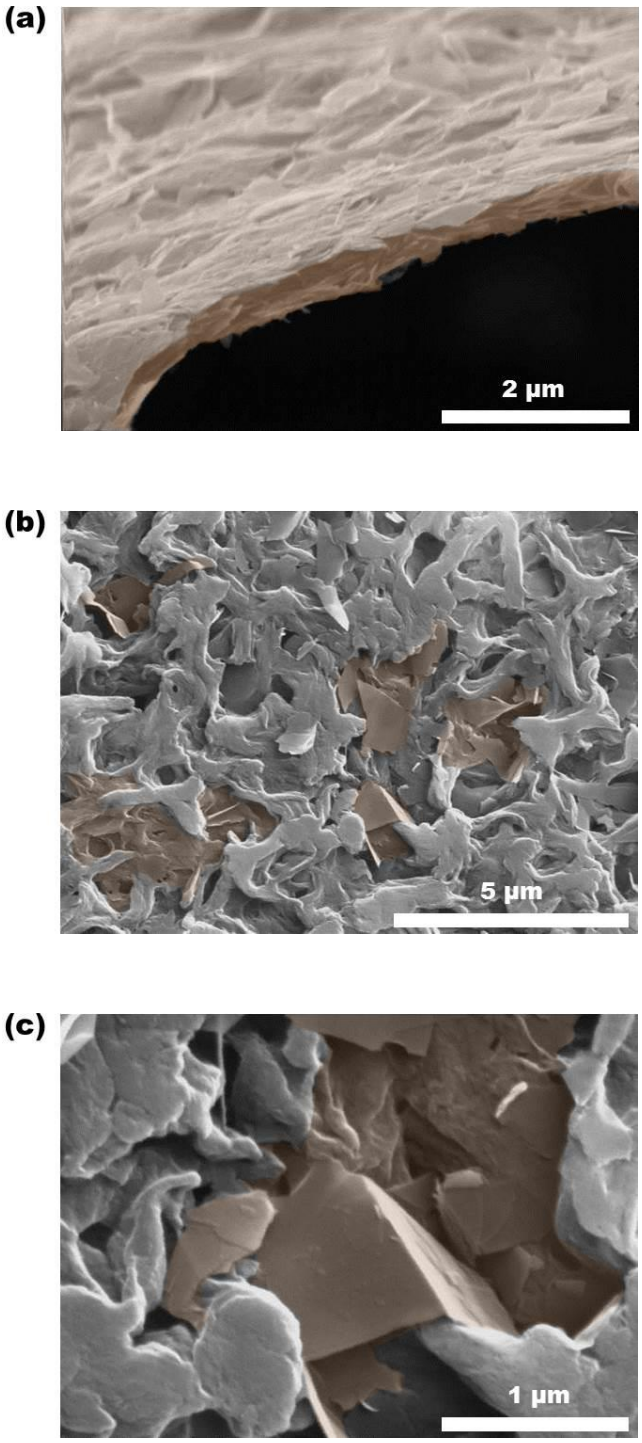

Figure 4.5 The graphene-based films through dry transfer process. (a) The representative graphene-based membranes with a thickness of 50 nm. (b) The surface of nylon filter demonstrating the randomly distributed residual graphene flakes and (c) its magnification of the residual graphene flakes.

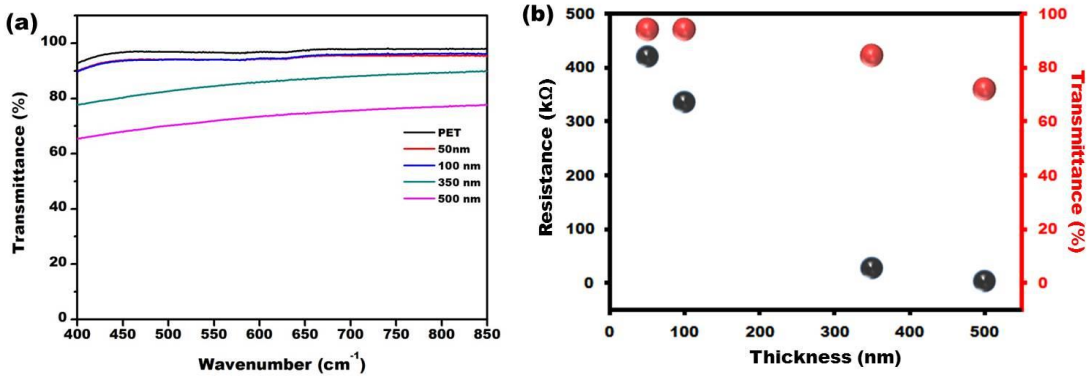

Figure 4.6 The transmittance and sheet resistance. (a) Transmittance of the graphene-based transparent electrodes on PET corresponding to different thickness. (b) The sheet resistance and transmittance properties according to different thickness of graphene-based membrane.

In **Figure 4.6**, the transmittance was measured by a UV-vis spectrometer according to the different thicknesses of graphene on PET. The corresponding average sheet resistance of the transferred graphene-based films measured using the four-point probe method was 421.1, 335.5, 27.7 and 3.6 kΩ cm^{-2} for thicknesses of the transferred graphene films of 50, 100, 350 and 500 nm, respectively, as shown in **Figure 4.6**a. Remarkably, the sheet resistance dropped dramatically to 421.1 and 3.6 kΩ cm^{-2} while maintaining the transmittance above 70%, which is attributable to the high interconnection between the high quality graphene platelets as demonstrated in **Figure 4.5**a. The conductance and transparency of our films are comparable to those made of graphene sheets formed by sonication of natural graphite in NMP. In order to demonstrate the transparency, the resulting graphene-based transparent electrodes on PET are shown in **Figure 4.7**, where one can see the Geisel Library at UC San Diego through the resulting transparent electrodes that have a transmittance of 84.5% with 27.7 kΩ cm^{-2}.

The 50 and 100 nm graphene films on PET had a transmittance of 84.5% and 71.9%, respectively.

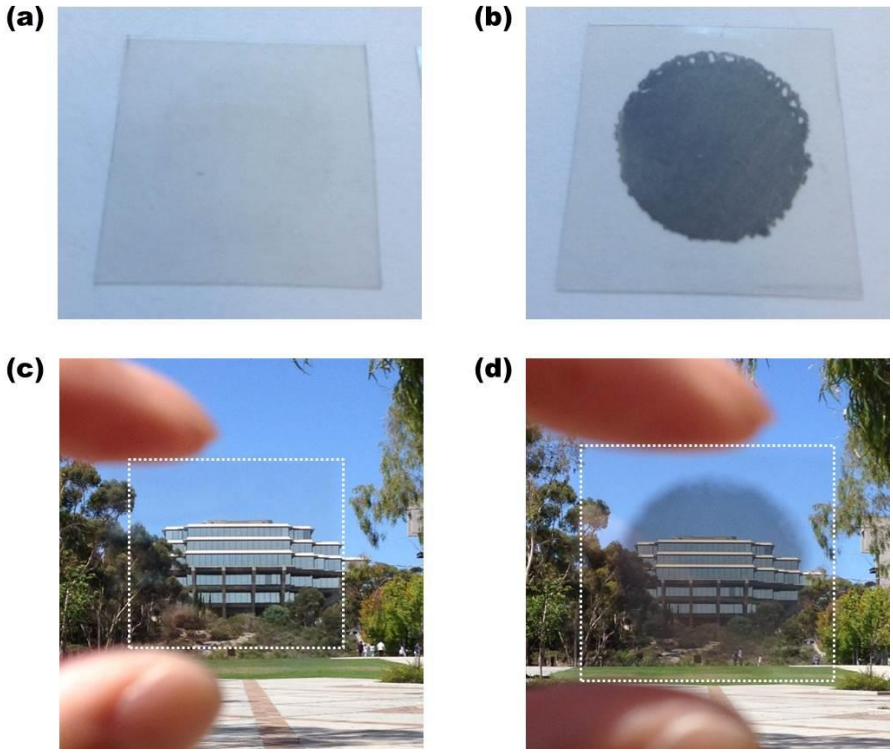

Figure 4.7 The transparent electrodes. (a) and (b) shows the transferred graphene-based membrane on PET films. (c) and (d) demonstrates the capability to see the Geisel Library at UCSD through the transparent electrodes.

4.4 Conclusion

In conclusion, the aqueous arc discharge produces graphene with high quality and less than 10 layers. The exfoliated graphene can be recollected by dispersion in NMP and filtration. In order to show the potential use as transparent electrodes, the collected graphene-based membranes were transferred to a PET substrate with high transparency (95% at 550 cm^{-1}) and low resistance (35 $k\Omega/cm^2$). These simple dry transfer methods

can also be applied to any desired substrate such as paper and glass.

Chapter 4, in part, has been submitted for publication in Nano Letters: Sejung Kim, Youngjun Song, Jennifer Marciniak, and Michael J. Heller, Bi- and trilayers graphene in an aqueous arc discharge process. The dissertation author was the primary investigator and author of this material.

4.5 References

1. Wang, X., Zhi, L. J., Tsao, N., Tomovic, Z., Li, J. L., Mullen, K. *Transparent carbon films as electrodes in organic solar cells.* Angew. Chem.Int. Ed. 2008, **47**: p. 2990-2992.

2. Wassei, J. K., Kaner, R. B. *Graphene, a promising transparent conductor.* Mater. Today 2010, **13**: p. 52-59.

3. Kim, J. Y., Lee, K., Coates, N. E., Moses, D., Nguyen, T. Q., Dante, M., Heeger, A. J. *Efficient tandem polymer solar cells fabricated by all-solution processing.* Science 2007, **317**: p. 222-225.

4. Wang, X., Zhi, L. J., Mullen, K. *Transparent, conductive graphene electrodes for dye-sensitized solar cells.* Nano Lett. 2008, **8**: p. 323-327.

5. De Arco, L. G., Zhang, Y., Schlenker, C. W., Ryu, K., Thompson, M. E., Zhou, C. W. *Continuous, highly flexible, and transparent graphene films by chemical vapor deposition for organic photovoltaics.* ACS Nano 2010, **4**: p. 2865-2873.

6. Su, Q., Pang, S. P., Alijani, V., Li, C., Feng, X. L., Mullen, K. *Composites of graphene with large aromatic molecules.* Adv. Mater. 2009, **21**: p. 3191-3195.

7. Bae, S., Kim, H., Lee, Y., Xu, X. F., Park, J. S., Zheng, Y., Balakrishnan, J., Lei, T., Kim, H. R., Song, Y. I., Kim, Y. J., Kim, K. S., Ozyilmaz, B., Ahn, J. H., Hong, B. H., Iijima, S. *Roll-to-roll production of 30-inch graphene films for transparent electrodes.* Nature Nanotechnol. 2010, **5**: p. 574-578.

8. Wu, Z. C., Chen, Z. H., Du, X., Logan, J. M., Sippel, J., Nikolou, M., Kamaras, K., Reynolds, J. R., Tanner, D. B., Hebard, A. F., Rinzler, A. G. *Transparent,*

conductive carbon nanotube films, Science 2004, **305**: p. 1273-1276.

9. Rowell, M. W., Topinka, M. A., McGehee, M. D., Prall, H. J., Dennler, G., Sariciftci, N. S., Hu, L. B., Gruner, G. *Organic solar cells with carbon nanotube network electrodes.* Appl. Phys. Lett. 2006, **88**: p. 233506.

10. Barnes, T. M., Bergeson, J. D., Tenent, R. C., Larsen, B. A., Teeter, G., Jones, K. M., Blackburn, J. L., van de Lagemaat, J. *Carbon nanotube network electrodes enabling efficient organic solar cells without a hole transport layer.* Appl. Phys. Lett. 2010, **96**: p. 243309.

11. Chiu, P. W., Kim, G. T., Gu, G., Philipp, G., Roth, S. *Electrical transport through carbon nanotube junction.* AIP Conf. Proc. 2001, **591**: p. 368.

12. Ho, G. W., Wee, A. T. S., Lin, J. *Electric field-induced carbon nanotube junction formation.* Appl. Phys. Lett. 2001, **79**: p. 260.

13. Tapaszto, L., Nemes-Incze, P., Osvath, Z., Darabont, A., Lambin, P., Biro, L. P. *Electron scattering in a multiwall carbon nanotube bend junction studied by scanning tunneling microscopy.* Phys. Rev. B 2006, **74**: p. 235422.

14. Bae, S., Kim, H., Lee, Y., Xu, X. F., Park, J. S., Zheng, Y., Balakrishnan, J., Lei, T., Kim, H. R., Song, Y. I., Kim, Y. J., Kim, K. S., Ozyilmaz, B., Ahn, J. H., Hong, B. H., Iijima, S. *Roll-to-roll production of 30-inch graphene films for transparent electrodes.* Nature Nanotechnol. 2010, **5**: p. 574-578.

15. Becerril, H. A., Mao, J., Liu, Z., Stoltenberg, R. M., Bao, Z., Chen, Y. *Evaluation of solution-processed reduced graphene oxide films as transparent conductors.* ACS Nano 2008, **2**: p. 463-470.

16. Eda, G., Fanchini, G., Chhowalla M., *Large-area ultrathin films of reduced graphene oxide as a transparent and flexible electronic material.* Nature Nanotechnol. 2008, **3**: p. 270-274.

17. Nair, R. R., Blake, P., Grigorenko, A. N., Novoselov, K. S., Booth, T. J., Stauber, T., Peres, N. M. R., Geim, A. K. *Fine structure constant defines visual transparency of graphene.* Science 2008, **320:** p. 1308.

18. Ludwig, A. W. W., Fisher, M. P. A., Shankar, R., Grinstein, G. *Integer quantum hall transition: An alternative approach and exact results.* Phys. Rev. B 1994, **50:** p. 7526.

19. Girifalco, L. A., Lad, R. A. *Energy of cohesion, compressibility, and the potential energy functions of the graphite system.* J. Chem. Phys. 1956, **25**: p. 693-697.

20. Parvez, K., Li, R., Puniredd, S. R., Hernandez, Y., Hinkel, F., Wang, S., Feng, X., Mullen, K. *Electrochemically exfoliated graphene as solution-processable, highly conductive electrodes for organic electronics.* ACS Nano 2013, **7**: p. 3598-3606.

Chapter 5: Water desalination

5.1 Introduction

The nanoporous two-dimensional (2D) graphene has been intensively investigated as a selective molecular barrier for the liquid- and gas-phase separation process for the purification of gas and water as well as for DNA sequencing through pores larger than the sizes of ions and molecules.[1-8] Recently, theoretical studies in membrane-based water desalination have revealed that the controllable permeability of 2D graphene has a superior efficiency than the current polymer-based filtration membranes to maximize ion selectivity.[9-12] Experimental studies have shown graphene-based materials to be promising candidates as ultimate membrane materials due to its mechanical stability to prevent breakdown,[12] its highly well-defined nanoporous structure to maximize the ion selectivity, and its ability to be made as thin as possible to maximize water flux.[13-15]

For nanofiltration of water, the Hagen-Poiseuille equation theoretically evaluates the mass flow through porous membranes per unit area as below:[1,16-19]

$$J = \frac{h^4 \cdot \Delta P}{12 \cdot L^2 \cdot \eta \cdot \Delta x} \qquad (1)$$

where h is the vertical space between adjacent graphene sheets, L is the average lateral length of the graphene sheets, η the viscosity of water (0.001 Pa s at 20 ℃), and Δx is the thickness of the graphene-based membrane. According to the equation (1), it is assumed that the liquid flows are basically based on laminar flow and zero-velocity at the boundary layer between the liquid and wall. In the case of graphitic nanostructure-based membranes, it shows that the enhancement of water flow is 2-4 orders of magnitude,

which is mainly attributed to the low interactions between water molecules and hydrophobic carbon wall.[17-19] Moreover, the graphene oxide-based membranes have a strong interaction with water molecules, which leads to the retention of water molecules on the graphene oxide sheets.[3,18,20] Thus, the non-oxidation regions of graphene were responsible for the high water flux.

Here, in this chapter, we produce multilayered graphene with less than 10 layers through an aqueous arc discharge, which can control the number of graphene layers and the degree of oxidation during the process. The graphene-based membranes are fabricated by vacuum-assisted filtration and show the practical potential for water purification, which is investigated by self-diffusion of ions and the rejection of organic dyes across the graphene-based membranes. Interestingly, the water flow rate and the salt rejection are found to be dependent on the degree of oxygen-related defects of the component graphene layers produced at various current levels between 1 and 4 A.

5.2 Experimental Section

5.2.1 Synthesis of graphene nanosheets by arc discharge in water

The schematic of the arc discharge in the water is illustrated in Figure SI 1 and the corresponding video is available in Video SI 1. High purity graphite electrodes used as anode (6 mm in diameter, 99.999%, Aldrich) and cathode (12 mm in diameter, 99.999%, Aldrich) were vertically aligned, and submerged in deionized water (18.2 MΩ). The two electrodes were connected to a DC power supply (Instek, SPS-3610). The anode is

moved up and down at 2 pps (pulse per second) to contact the fixed cathode with application of a voltage (25 V) to initiate arc discharge. Currents were controlled at around 1 A. Once the graphene layers are produced by the arc discharge in water, the graphene platelets migrate towards the surface of the water and laterally assemble into large graphene-based films. The graphene-based films were collected by dipping a silicon wafer or a TEM grid into the water and dried in a convection oven over night for characterization.

5.2.2 Fabrication of the graphene-based membrane for water desalination

The produced graphenes were collected with a nylon membrane (EMD Millipore, 0.45 μm) by vacuum filtration and washed with water several times. Then, the collected graphenes were dispersed in N-methyl-2-pyrrolidone (NMP) by sonication for 5 minutes in order to prevent further exfoliation. The dispersed graphene solution stands over-night in order to separate the multi-layered graphene. The resulting graphene solution was recollected with a nylon membrane as a supporting substrate by vacuum filtration followed by drying over night at 85 ℃. A piece of graphene-based membrane with a nylon membrane was assembled with aluminum foil tape containing a hole (2.5 mm in diameter).

5.2.3 Transport Measurement

The self-diffusive permeation experiments were carried out using homemade 20

mL side-by-side diffusion cells, as indicated in Supplementary Figure X. Briefly, a piece of graphene-based membrane with a nylon membrane was inserted between the source cell (ions in DI water) and the drain cell (only DI water) and sealed with a rubber O-ring following pressing together of the both cells. For the permeation experiments, 20 mL of a 0.5 M ion solution and DI water were injected into the source and drain cells, respectively, at the same speed in order to prevent hydrostatic pressure gradients, followed by magnetically stirring both solutions to avoid ion concentration gradients. During the ion permeation process, 0.5 mL of the source solution and the permeated solution were taken in order to monitor the permeation progress and to avoid external hydrostatic pressures across the membrane. In order to analyze the permeated ions, ICP-OES was carried out to monitor the permeated cation ions and a UV-vis spectrometer was used to monitor the amount of permeated organic dyes.

5.2.4 Characterization

The morphology is observed with scanning electron microscopy (SEM, HITACHI S-XX) operated at 10 kV and transmission electron microscopy (TEM, FEI Tacnai G2) with an accelerating voltage of 200 kV. X-ray photoelectron spectroscopy (XPS) measurements were performed on an ESCA-LAB 250 photoelectron spectrometer. C1s and O1s peaks were analyzed. Raman spectra were measured and collected using a 512 nm laser by a Lab RAM HR800. The UV-vis spectra were performed using Shimadzu UV-3600 spectrometer with correction for solvent background. Atomic force microscopy (AFM, Dimension 3100 Veeco) was performed in tapping mode with a Si tip (resonance

frequency = 320 kHz; spring constant = 42 N/m) For transmission electron microscopy analysis, graphene dispersion was drop-casted onto a carbon-coated copper grid and imaged in high vacuummode. The I-V measurements were performed by a Hewlett-Packard 4156B semiconductor parameter analyzer under ambient conditions.

5.3 Results and Discussion

The graphene-based nanofiltration for water filtration is based on the permeation of water molecules through the intrinsic holes and affinity to water and ions of graphene layers. Therefore, it is assumed that water filtration is achieved when the water molecules migrate through the two-dimensional (2D) nanocapillaries between the stacked graphene sheets and the intrinsic holes on graphene layers. In addition, the ions are assumed to be either blocked by the oxygen-related functional groups, or their movement interrupted by the strong interactions between the hydrated ions and carbon walls, as illustrated in **Figure 5.1**a.

Our graphene-based membranes were simply prepared by assisting vacuum filtration of the highly diluted graphene dispersions on commercial microfiltration membranes (polyamide membranes (PA), 0.45 μm in pore size), which were used as a supporting substrate (**Figure 5.1**b). The thickness of the assembled graphene-based membranes was controlled by the amount of graphene dispersion and the representative membranes that have a thickness of ~200 nm are shown in **Figure 5.1**c. The component graphene sheets of the membranes were produced by an arc discharge process we developed in a previous study that can produce a controlled stacked number of graphene

layers and degree of oxidation by adjusting the current level during the arc discharge.[21]

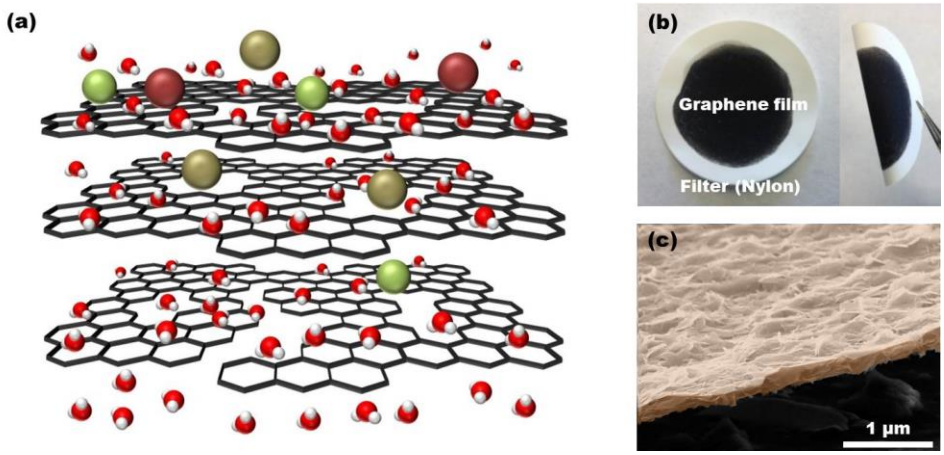

Figure 5.1 Water desalination process through graphene-based membrane. (a) Schematic illustration of water desalination by size selective diffusion. (b) The resulting graphene-based membranes on a commercial polyamide membrane. (c) SEM image of the representative graphene-based membranes with a thickness of 50 nm.

In short, the aqueous arc discharge process is composed of two graphite electrodes submerged in DI water as a dielectric medium followed by application of a voltage (25 V) across two electrodes. The produced graphene was characterized by transmission electron microscopy (TEM), atomic force microscopy (AFM), and X-ray photoemission spectroscopy (XPS) in order to investigate the intrinsic properties of graphene in our system for water desalination. The produced graphene has two and three layers at 1 A and multilayers (4-7 layers) at 4 A, as shown in **Figure 5.2**a and b, with the same interlayer distance (~0.35 nm) of that of pristine graphene. The number of stacked graphene layers was analyzed by using AFM. The representative AFM image is shown in **Figure 5.3**a and the produced graphene appears to be flat and wrinkled thin sheets on the substrate with ~ 1.399 nm thickness. The distribution of the number of graphene layers is more than 70 %

less than 10 layers: bi- and tri-layers of graphene are 73 % at 1 A, and 4- to 7-layered graphene is 78% at 4 A, as shown in **Figure 5.2**b.

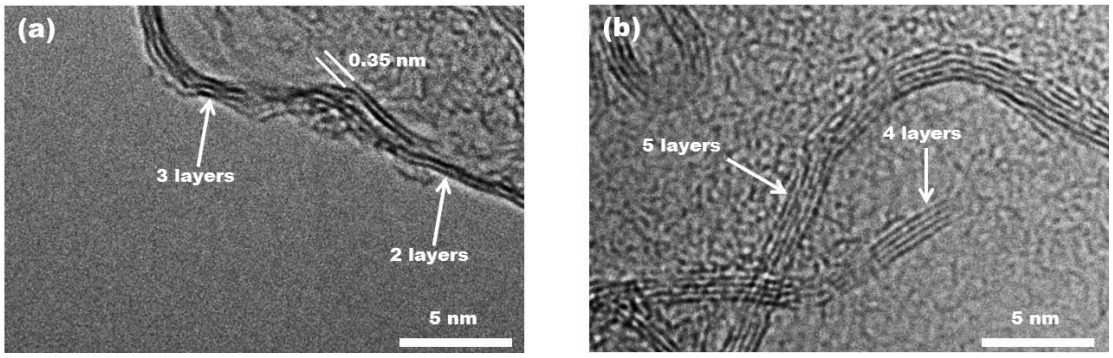

Figure 5.2 Morphological characterization with TEM. (a) The exfoliated graphene produced at 1 A composed of bi- and three-layers of graphene with a interlayer distance of 0.35 nm. (b) The exfoliated graphene produced at 4 A composed of four- and five-layers of graphene.

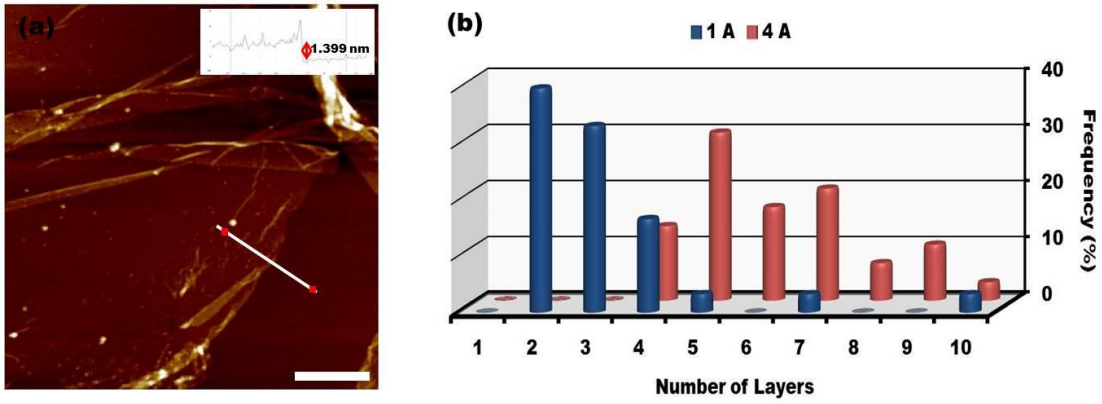

Figure 5.3 The distribution of the graphene layers. (a) The representative AFM image of the exfoliated graphene produced at 1 A with a height of 1.399 nm. (b) The distribution of the number of graphene layers produced at 1 A and 4 A.

The intrinsic properties of an aqueous arc discharge with graphite electrodes produce reactive species such as O^{+}, O^{++}, and H^{+} followed by CO/CO_2 gas and oxidation of graphene.[21-24] The reactive species are proportionally produced according to the arc discharge power, which might leads to the controllable degree of oxidation of graphene. In order to estimate the degree of oxidation, X-ray photoelectron spectroscopy (XPS) was carried out on the produced graphene at 1 A (Gr1A) and 4 A (Gr4A), respectively. The wide-scan XPS spectra are show in Figure SI2 and the peaks appear at 284.90 eV and 532.90 eV for C1s and O1s, respectively. In order to compare the oxidation degree of graphene, deconvolution of high-resolution C1s XPS spectrum were performed for Gr1A and Gr4A, as shown in **Figure 5.4**. Deconvolution of the spectra of C1s indicates that non-oxygenated carbon atoms (284.5 eV) were decreased with the current level from Gr1A to Gr4A. Otherwise, oxygenated carbon atoms such as C-O (286.2 eV), O-C=O (288.5 eV) were increased from 28.1 % (Gr1A) to 53.9% (Gr4A). According to the XPS results of oxygenated carbon atoms, the aqueous arc discharge can control the oxidation degree of graphene by adjusting the current level during the process.

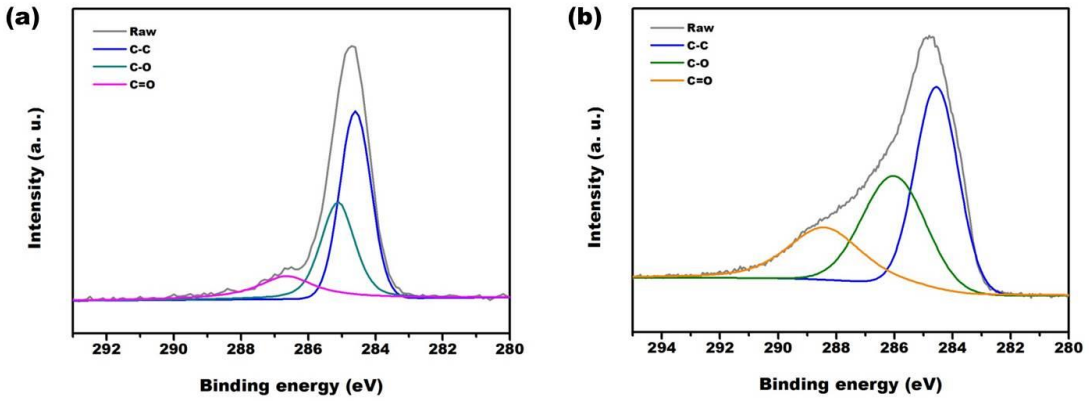

Figure 5.4 High resolution of C1s XPS spectrum. (a) Deconvolution of the spectra of C1s for Gr1A. (b) Deconvolution of the spectra of C1s for Gr4A.

In order to investigate the water purification performance, the two different homemade devices were assembled in order to measure water transport performance and self-diffusion of ions through graphene-based membranes corresponding to the different amount of oxygen-related functional groups on the graphene produced at different current levels.

First, the water transport performance was evaluated by assembling the device, which is composed of one container filled with water (10 mL) on top and another container with a hole to equilibrate the atmospheric pressure during transportation of water through the membranes, as shown in **Figure 5.5**.

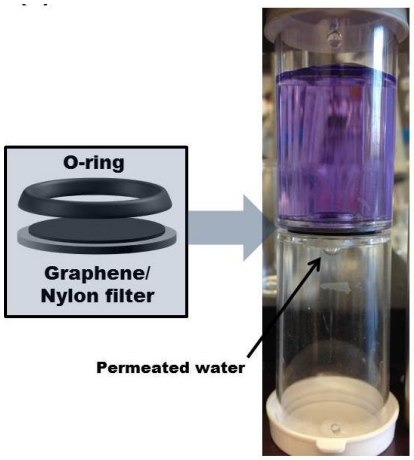

Figure 5.5 The schematic illustration for the Arrhenius behavior of water flow through graphene-based membranes.

The graphene-based membranes were inserted between the two containers and sealed with an O-ring, then, the water on top comes in contact with the membranes. Using temperature, the vapor pressure was increased from 2.33 to 31.09 kPa, which water was pushed by increased water vapor pressures. As a control, the polyamide (PA) only

(0.45 μm pore diameter) was tested with the same configuration as the device, and the measured water flux was in the range of 1.6 to 437.0 L h^{-1} bar^{-1} m^{-2}, as shown in **Figure 5.6**a and b. The graphene-based membranes were fabricated for water transportation with different thicknesses of 200, 850 and 1120 nm. The fluxes were monitored for an hour. It was found to be increased with increasing temperatures, with the highest water fluxes of 362.3, 345.8 and 330.6 L h^{-1} bar^{-1} m^{-2} at 70 ℃ with thicknesses of 200, 850 and 1120 nm, respectively. At a constant thickness of graphene-based membranes, the water flux proportionally increased with increasing temperature. As demonstrated in **Figure 5.6**b, the water flux with a thickness of 200 nm showed the highest water flux 362.3, which is a comparably high water flux value with commercial desalting membranes: UTC60 is 15.4 L h^{-1} bar^{-1} m^{-2}.[25] In addition, the resulting water flux value is also comparable with that of a graphene oxide-based membrane reported recently (711 L h^{-1} bar^{-1} m^{-2}).[18,19] Theoretically, according to the equation (1), for the thickest of our graphene-based membranes (Δx = 1120 nm), the water flux of x L h^{-1} bar^{-1} m^{-2},is x orders of magnitude smaller than our experimental results (L h^{-1} bar^{-1} m^{-2}).[16,18]

This high water flux is ascribed to the low interaction between the water molecules and carbon walls, which leads to the single file of water molecules by ordered hydrogen bonds.[26-28] In addition, the low contents of oxygen on our graphene components in the membrane have nanocapillaries that are in 2D forms. Interestingly, the oxygen-related functional groups on the graphene layers might hinder water transport in the graphene due to the strong interactions (hydrogen bonding) between them; this is furthermore demonstrated by the fact that the graphene oxide-based membranes have been found to have half the water flux at the same conditions.[17,18,29-31]

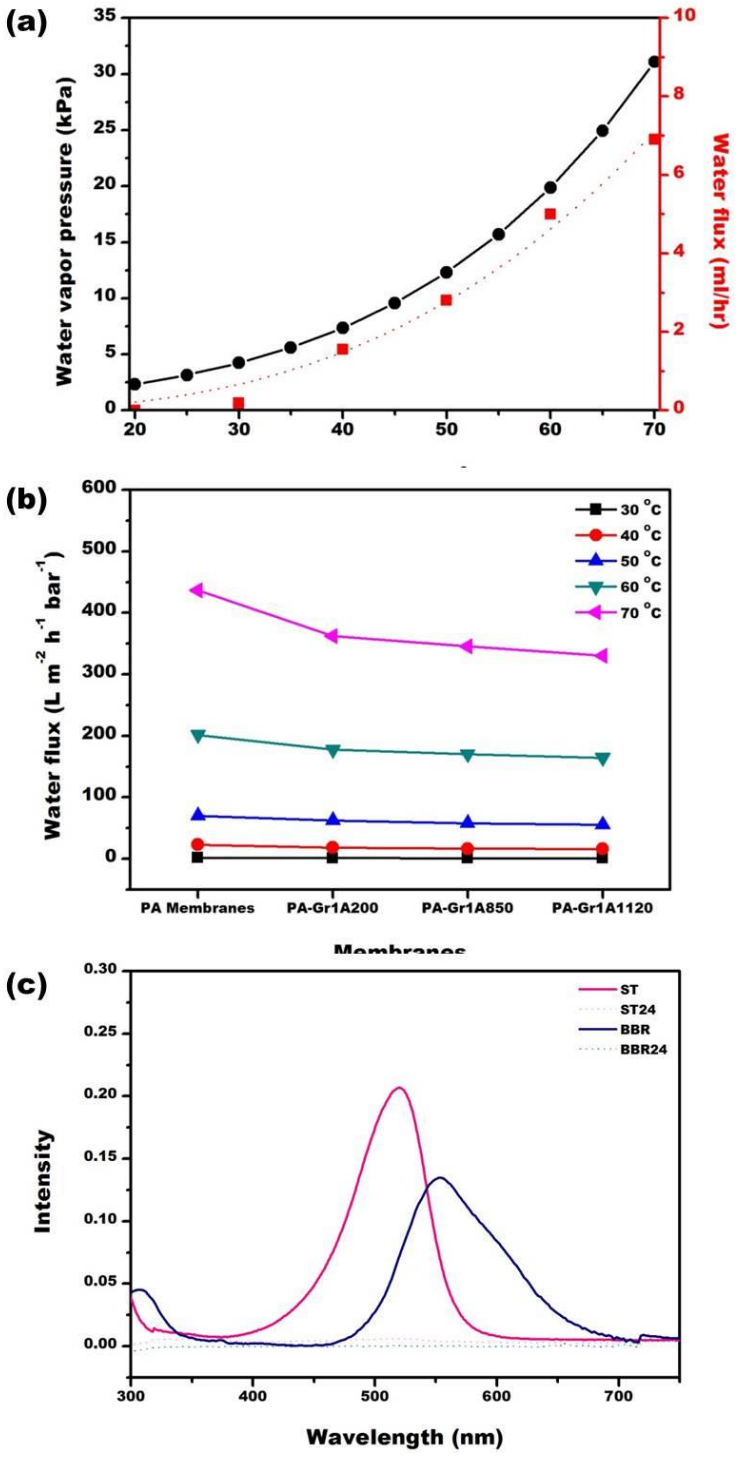

Figure 5.6 The schematic illustration for the Arrhenius behavior of water flow through graphene-based membranes. (a) Water flux with temperature through PA membranes. (b) The water flux with thicknesses with temperature. (c) UV-vis spectrum of permeate organic dye through graphene-based membranes.

In order to verify the assumption, the hydrophilic organic dyes were transported through the membranes, such safranin T (ST) and brilliant blue R (BBR) at a concentration of 10 μM. As shown in Figure x, the filtration measurement for organic dyes of ST and BBR were carried out under the pressure-driven filtration at relatively low pressure (at 40 ℃), followed by measurement of the concentration of permeate solutions. In **Figure 5.6**c, both ST and BBR were not detected in the permeate solutions by comparing the absorption intensity through a UV-vis spectrometer. According to the chemical structure of graphene and organic dyes, the lack of permeability of the organic dyes could possibly be attributed to the π-π interactions between the dyes and the graphene, leading to the direct absorption of dyes into the graphene layers.

Second, the self-diffusion of ions through graphene-based membranes was evaluated by constructing another homemade device, as shown in **Figure 5.7**a. The graphene-based membranes were inserted in the middle of two containers and sealed with an O-ring: one side of container was filled with 20 mL of 500 mM sodium chloride (NaCl) solution (the source solutions) and the opposite side of the container was filled with the same volume of DI water (the drain solutions). In order to prevent concentration gradients, the two solutions were magnetically stirred. During the diffusion of ions through membranes, 100 μL of the source and the drain solutions were removed every 30 min, and diffusion rates were calculated by measuring the drain solutions with a conductivity meter and ICP-OES for conductivity and cation values, respectively.

In **Figure 5.7**b, the measured conductivities of permeates of the NaCl solutions are plotted for all membranes such as PA membranes, Gr1A, and Gr4A membranes. For the thickness of 200 nm, the permeate conductivity through Gr1A- and Gr4A-based

membranes was decreased by 67.7% and 64.5%, respectively, at 120 min for comparison with the PA membranes.

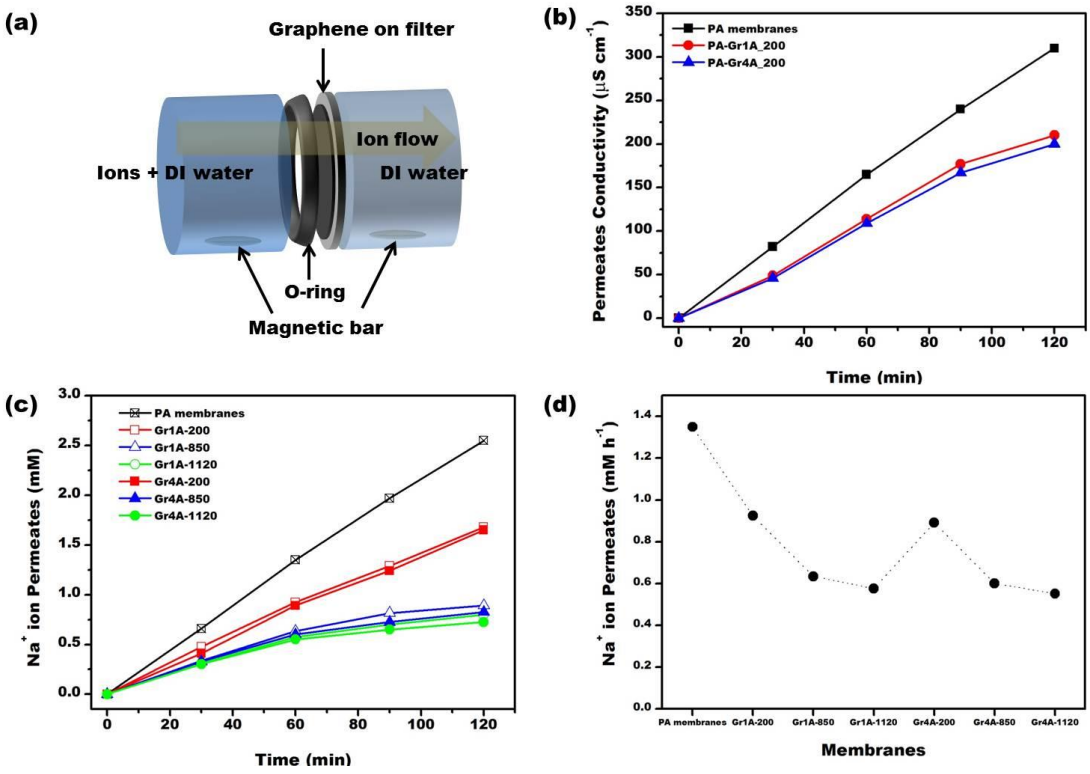

Figure 5.7 The ion diffusion through graphene-based membranes. (a) The schematic illustration for the ions diffusion through graphene-based membranes. (b) The ion diffusion rate through graphene-based membranes by using a concentration fo 500 mM NaCl solution, where are consisted of the exfoliated graphene produced at 1 A and 4 A, respectively. (c) and (d) show the Na^+ ion permeation rate through graphene-based membranes with thicknesses.

For an accurate Na^+ concentration, it was measured with ICP-OES and there is a linear relationship between the conductivity and concentration of Na^+. In **Figure 5.7**c, the change in transported ion concentration indicates that the permeability of the Na^+ was

proportionally increased. However, the thickness of graphene-based membranes has blocked the transportation of ions through membranes. In the case of Gr1A, the Na^+ ions decreased from 0.92 mM h^{-1} to 0.63 and 0.58 mM h^{-1} for thicknesses of 850 and 1120 nm, respectively. Similarly, the concentration of Na^+ ions decreased from 0.89 mM h^{-1} to 0.60 and 0.55 mM h^{-1} for thicknesses of 850 and 1120 nm of Gr4A, respectively.

The results, in **Figure 5.7**d, reveal that the ion permeations have similar tendencies according to the thickness of the graphene-based membranes and diffusion time for Gr1A and Gr4A. However, as the amount of oxygen-related functional groups was increased, the Gr4A-based membranes show a higher efficiency for ions retention than that of Gr1A. For the same thickness of membranes, the controllable degree of graphene oxidation is 28.1 % (Gr1A) to 53.9% (Gr4A), for water purification, the permeation efficiency of Gr4A-based membranes is slightly smaller than that of Gr1A, in the range of 94% and 96%. More importantly, the hydrophobic portion of graphene can facilitate water permeation, but the oxygen-related functional groups can block ion permeation, which leads to the high salt rejection efficiency along with high water permeation rates.

5.4 Conclusion

In conclusion, we have developed a novel aqueous arc discharge process to produce graphene with a controllable number of oxygen-related functional groups on graphene sheets. The ultrathin graphene-based membranes were fabricated from different amounts of oxygen on graphene by a vacuum-assisted assembly process. The graphene sheets compactly stack on each other, constructing well-defined 2D nanochannels, and

the hydrophobic carbon nanochannels favor high water flux and show excellent performance for retention of organic dyes based on the mechanisms of physical sieving and hydrophobic interaction. Otherwise, Gr4A with high numbers of oxygen on graphene sheets has an excellent ion retention compared to bare polyamide membranes, which are highly affected by interactions at the water-graphene interface leading to lowering friction between hydrophobic surface and water, preventing hydrogen bonding. Further improvement of graphene-based nanofiltration might include optimizing the size and density of holes on the graphene sheets, adjusting the space between graphene sheets, and increasing the antifouling property by chemical modification.

5.5 References

1. R. R. Nair, H. A. Wu, P. N. Jayaram, I. V. Grigorieva, A. K. Geim, *Unimpeded permeation of water through helium-leak-tight graphene-based membranes.* Science 2012, **335**: p. 442-444.
2. S. P. Koenig, L. Wang, J. Pellegrino, J. S. Bunch, *Selective molecular sieving through porous graphene.* Nature Nanotechnol. 2012, **7**: p. 728-732.
3. R. K. Joshi, P. Carbone, F. C. Wang, V. G. Kravets, Y. Su, I. V. Griforieva, H. A. Wu, A. K. Geim, R. R. Nair, *Precise and ultrafast molecular sieving through graphene oxide membranes.* Science 2014, **343**: p. 752-754.
4. H. Li, Z. Song, X. Zhang, Y. Huang, S. Li, Y. Mao, H. J. Ploehn, Y. Bao, M. Yu, *Ultrathin, molecular-sieving graphene oxide membranes for selective hydrogen separation.* Science 2013, **342**: p. 95-98.
5. H. W. Kim, H. W. Yoon, S. –M. Yoon, B. M. Yoo, B. K. Ahn, Y. H. Cho, H. J. Shin, H. Yang, Y. Paik, S. Kwon, J. –Y. Choi, H. B. Park, *Selective gas transport through few-layered graphene and graphene oxide membranes.* Science 2013, **342**: p. 91-95.
6. D. Jiang, V. R. Cooper, S. Dai, *Porous graphene as the ultimate membrane for gas separation.* Nano Lett. 2009, **9**: p. 4019-4024.

7. S. Garaj, W. Hubbard, A. Reina, J. Kong, D. Branton, J. A. Golovchenko, *Graphene as a subnanometer trans-electrode membrane.* Nature 2010, **467**: p. 190-194.

8. G. F. Schneider, S. W. Kowalczyk, V. E. Calado, G. Pandraud, H. W. Zandbergen, L. M. K. Vandersypen, C. Dekker, *DNA translocation through graphene nanopores.* Nano Lett. 2010, **10**: p. 3163-3167.

9. K. Sint, B. Wang, P, Král, *Selective ion passage through functionalized graphene nanopores.* J. Am. Chem. Soc. 2008, **130**: p. 16448-16449.

10. G. Tocci, L. Joly, A. Michaelides, *Friction of water on graphene and hexagonal boron nitride from ab initio methods: very different slippage despite very similar interface structures.* Nano Lett. 2014, **14**: p. 6872-6877.

11. D. Cohen-Tanugi, J. C. Grossman, *Water desalination across nanoporous graphene.* Nano Lett. 2012, **12**: p. 3602-3608.

12. D. Cohen-Tanugi, J. C. Grossman, *Mechanical strength of nanoporous graphene as a desalination membrane.* Nano Lett. 2014, **14**: p. 6171-6178.

13. S. C. O'Hern, C. A. Stewart, M. S. H. Boutilier, J. –C. Idrobo, S. Bhaviripudi, S. K. Das, J. Kong, T. Laoui, M. Atieh, R. Karnik, *Selective molecular transport through intrinsic defects in a single layer of CVD graphene.* ACS Nano, 2012, **6**: p. 10130-10138.

14. S. C. O'Hern, M. S. H. Boutilier, J. –C. Idrobo, Y. Song, J. Kong, T. Laoui, M. Atieh, R. Karnik, *Selective ionic transport through tunable subnanometer pres in single-layer graphene membranes.* Nano Lett. 2014, **14**: p. 1234-1241.

15. S. C. O'Hern, D. Jang, S. Bose, J. –C Idrobo, Y. Song, T. Laoui, J. Kong, R. Karnik, *Nanofiltration across defect-sealed nanoporous monolayer graphene.* Nano Lett. 2015, **15**: 3254-3260.

16. J. K. Holt, H. G. Park, Y. Wnag, M. Stadermann, A. B. Artyukhin, C. P. Grigoropoulos, A. Noy, O. Bakajin, *Fast mass transport through sub-2-nanometer carbon nanotubes.* Science 2006, **312**: p. 1034-1037.

17. M. Majumder , N. Chopra , B. J. Hinds, *Mass transport through carbon nanotube membranes in three different regimes: ion diffusion and gas and liquid flow.* ACS Nano 2011, **5**: p. 3867-3877.

18. Y. Han, Z. Xu, C. Gao, *Ultrathin graphene nanofiltration membrane for water purification.* Adv. Funct. Mater. 2013, **23**: p. 3693-3700.

19. H. Huang, Z. Song, N. Wei, L. Shi, Y. Mao, Y. Ying, L. Sun, Z. Xu, X. Peng, *Ultrafast viscous water flow through nanostrand-channelled graphene oxide membranese.* Nature Commun. 2013, **4**: p. 2979.

20. P. Sun, Q. Chen, X. Li, H. Liu, K. Wang, M. Zhong, J. Wei, D. Wu, R. Ma, T. Sasaki, H. Zhu, *Highly efficient quasi-static water desalination using monlayer graphene oxide/titania hybrid liminates.* NPG Asia Mater. 2015, **7**: p. e162.

21. S. Kim, Y. Song, T. Takahashi, T. Oh, M. J. Heller, *An aqueous single reactor arc discharge process for the synthesis of graphene nanosphres.* Small 2015, **11**: p. 5041-5046.

22. P. T. Eubank, M. R. Patel, M. A. Barrufet, B. Bozkurt, *Theoretical models of the electrical discharge machining process. III. The variable mass, cylindrical plasma model.* J. Appl. Phys. 1993, **73**: p. 7900-7909.

23. N. Sano, H. Wang, I. Alexandrou, M. Chhowalla, K. B. K. Teo, G. A. J. Amaratunga, *Properties of carbon onions produced by an arc discharge in water.* J. Appl. Phys. 2002, **92**: p. 2783-2788.

24. N. Sano, H. Wang, M. Chhowalla, I. Alexandrou, G. A. J. Amaratunga, *Synthesis of carbon 'onions' in water.* Nature 2001, **414**: p. 506-507.

25. K. O. Agenson , J. I. Oh , T. Urase, *Retention of a wide variety of organic pollutants by different nanofiltration/reverse osmosis membranes: controlling parameters of process.* J. Membr. Sci. 2003, **225**: p. 91-103.

26. J. T. Paci, T. Belytschko, G. C. Schatz, *Computational studies of the structure, behavior upon heating, and mechanical properties of graphite oxide.* J. Phys. Chem. C 2007, **111**: p. 18099-18111.

27. K, Erickson, R. Erni, Z. Lee, N. Alem, W. Gannett, A. Zettl, *Determination of the local chemical structure of graphene oxide and reduced graphene oxide.* Adv. Mater. 2010, **22**: p. 4467-4472.

28. C. Mattevi, G. Eda, S. Agnoli, S. Miller, K. A. Mkhoyan, O. Celik, D. Mostrogiovanni, G. Granozzi, E. Garfunkel, M. Chhowalla, *Evolution of electrical, chemical, and structural properties of transparent and conducting chemically derived graphene thin films.* Adv. Funct. Mater. 2009, **19**: p. 2577-2583.

29. G. Hummer , J. C. Rasaiah , J. P. Noworyta, *Water conduction through the hydrophobic channel of a carbon nanotube.* Nature 2001, **414**: p. 188-190.

30. S. Joseph, N. R. Aluru, *Why are carbon nanotubes fast transporters of water.* Nano Lett. 2008, **8**: p. 452-458.

31. H. Y. Yang, z. J. Han, S. F. Yu, K. L. Pey, K. Ostrikov, R. Karnik, *Carbon nanotube membranes with ultrahigh specific adsorption capacity for water desalination and purification.* Nature Commun. 2013, **4**: p. 2220.

Chapter 6: A seamless process for crumpling graphene into nanospheres

6.1 Introduction

The ability to manipulate the three-dimensional (3D) architecture of graphene is desirable for introducing unique properties that improve the performance of the materials for applications in energy generation/storage,[1-4] composites,[5-7] biomedicine[8] and environment.[9] The elasto-plastic properties of graphene can be irreversibly deformed into 3D structures by means of applied compressive force to generate ridges and vertices on two-dimensional (2D) graphene sheets.[10-12] The plastically deformed ridges can stabilize the individual particles and prevent them from forming restacked aggregates, which are the major drawback of 2D nanostructure due to their strong van der Waals attractions.[13-15] In the case of the plastic deformation, 2D graphene sheets ideally avoid interaction with other graphene sheets (self-avoidance) and the confinement force generates the crumpled 3D structure. The force to crumple 2D graphene sheets is governed by the fractal scaling law by[11,12,14]

$$M \propto {R_M}^D \quad (1)$$

where M is the mass of the 2D graphene sheet, R_M is the crumpled particle diameter, and D is the fractal dimension of the crumpled particles. D varies as $2 \leq D \leq 3$, where $D = 2$ is a flat sheet, $D = 3$ is a sphere, and $D = 2.5$ is for self-avoiding sheets. Several synthetic methods to produce crumpled 3D graphene particles from 2D sheets have been developed which include aerosol pyrolysis,[3,4,9,13-15] microwave,[1] and substrate regulation.[7]

In the case of the aerosol pyrolysis, water-soluble graphene oxide (GO) is irreversibly deformed into a crumpled 3D architecture despite the high Young's modulus

(207.6 ± 23.4 GPa for monolayer of GO).[14,15] In this process, the aqueous GO dispersion was atomized into fine droplets causing their rapid evaporation, which induces capillary compressive forces that produce the crumpled GO particles. A recent study has demonstrated the proportional relationship between the evaporation rate and the confinement force that induces the morphological transition of 2D graphene into 3D structural particles.[15] With this morphological transition strategy, the resulting crumpled graphene oxide spheres show highly aggregation-resistive properties that allows their dispersion in common solvents without chemical functionalization. The particles remain individually dispersible even after high-pressure compression results in higher specific surface area.[13] While the aerosol pyrolysis process is relatively simple, the resulting particles have intrinsic problems that include poor electrical conductivity due to residual oxygen in the basal plane and the edges of graphene even after further chemical or thermal reduction processes.[17,18]

6.2 Experimental Section

6.2.1 Synthesis of crumpled graphene nanospheres

The schematic of the arc discharge apparatus is shown in **Figure 6.1**. High purity graphite electrodes were aligned vertically and used as the cathode (6 mm in diameter, 99.999%, Aldrich) which moves up and down at 2 pps (pulse per second) to contact the fixed anode (12 mm in diameter, 99.999%, Aldrich). Both electrodes were connected to a DC power supply (Instek, SPS-3610) and submerged in deionized water (18.2 M**Ω**). The

initial voltage and current were 25 V and ~4 A. N_2 gas was continuously supplied into the water to purge O_2 out. Once the graphene nanosheets were produced by the arc discharge in the water, the particles floated to the surface of the water and self-assembled into large graphene films. To produce crumpled graphene balls, toluene was supplied into a surfactant soultion (1% w/v, polyvinylpyrrolidon, Mw ~50k) as a dispersed phase in O/W emulsions at rates ranging from 100 µl/hr to 600 µl/hr. With the same arc discharge procedure as before, graphene sheets and particles were produced.

6.2.2 Characterization

The exfoliated graphene nanosheets were characterized by Raman spectroscopy using a 514 nm laser (Renishaw, inVia Raman microscope) in order to evaluate the number of the exfoliated graphene layers. In addition, atomic force microscopy (AFM) images of graphene sheets were taken in tapping mode using a SPM Dimension 3100 from Veeco. Moreover, the specimen of graphene nanosheets were observed by the optical microscopy. The morphological structure was observed by scanning transmission electron microscopy (STEM, using HITACHI STEM facility) and cryo-electron microscopy (FEI, Tecnai G^2 Sphera). The chemical composition was investigated by x-ray photoemission spectroscopy (XPS, AXIS Nova), followed by estimating the defects in the graphenes.

6.3 Results and Discussion

A schematic representation of the aqueous single reactor arc discharge process to produce 3D CGrSs is shown in **Figure 6.1**. The arc discharge was initiated by bringing in contact and separating the two graphite electrodes submerged in DI water followed by applying the voltage (25 V). Toluene was supplied as a dispersed phase at the injection rate of 600 µl/hr to form O/W emulsions through a hole inside the bottom anode into a water solution containing polyvinylpyrrolidone (Mw ~50k) at a concentration of 1% w/v.

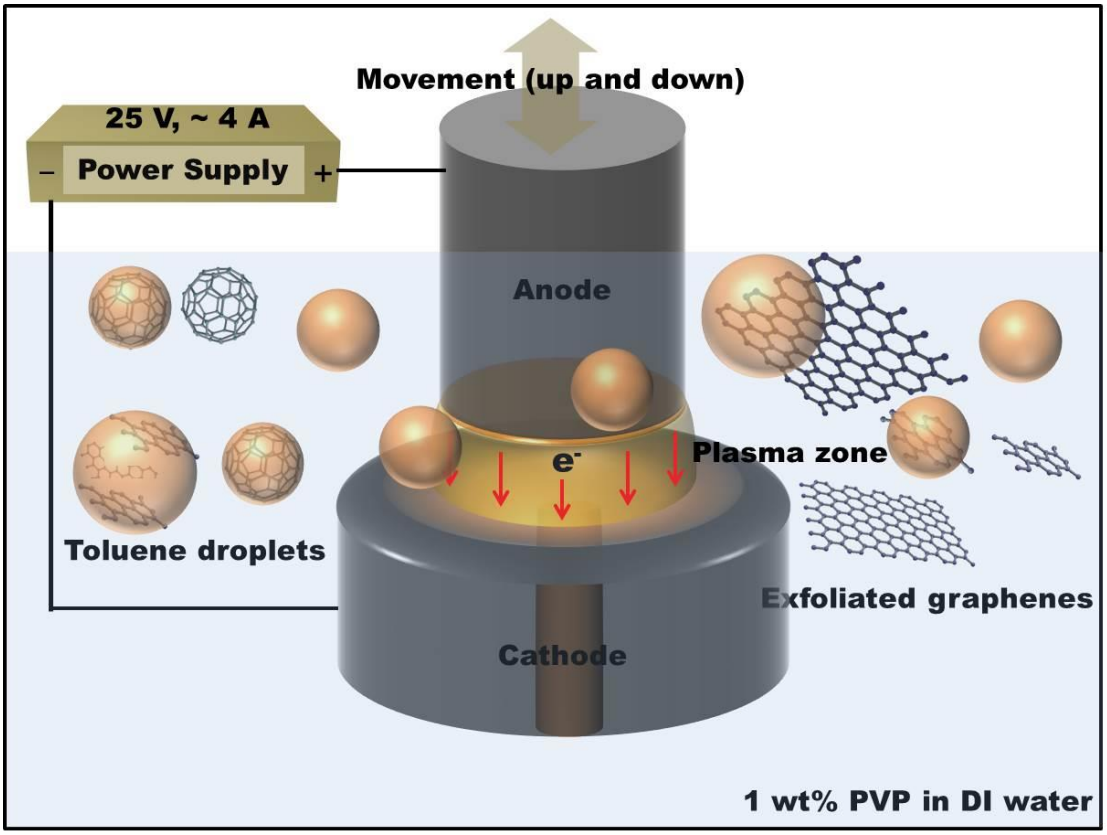

Figure 6.1 Schematic illustration of the experimental setup for the aqueous single reactor arc discharge process for crumpling 2D multi-layered graphenes (MLGs). by adopting toluene droplets. The inset shows an image of the exfoliated highly wrinkled 2D MLGs by scanning transmission electron microscopy (STEM) without toluene droplets (scale bar: 3 µm).

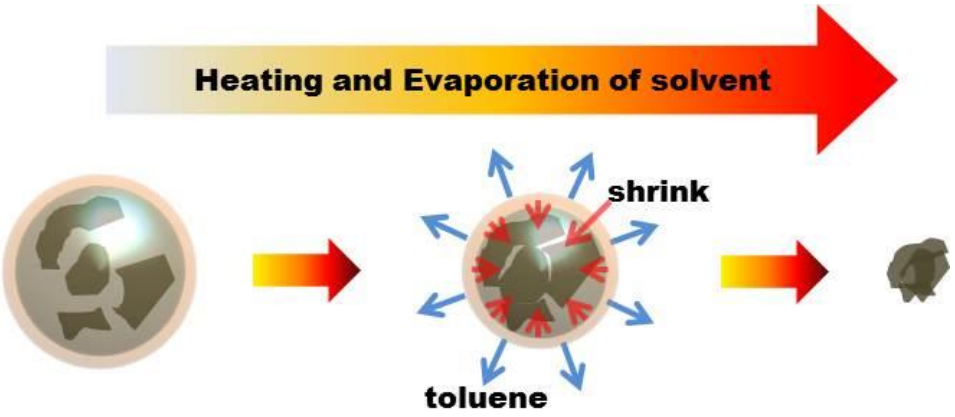

Figure 6.2 Schematic illustration of the crumpling process. The exfoliated graphene are entrapped by oil-in-water emulsion and the crumpling process occurred by evaporation of toluene.

Subsequently, as shown in **Figure 6.2**, the O/W emulsion can encapsulate the 2D MLGs inside the toluene droplets or the interface between toluene and water depending on the difference in the solvation energy and the hydrophobic properties of the graphene layers. The O/W emulsions can exert significant force to induce the deformation of the entrapped graphene producing higher curvatures.[16] The deformation of the 2D MLGs is accelerated as toluene is evaporated by heating from the arc discharge process followed by capillary compression. **Figure 6.3** shows the resulting sphere-like particles which have about a 600 nm diameter with a crumpled/wrinkled surface. In addition, the spherical particle has a hollow structure consisting of crisscrossing ridges on a smooth thin surface layer. The combination of O/W emulsion and the arc discharge process produces unique morphological distinct individual 3D CGrSs particles.

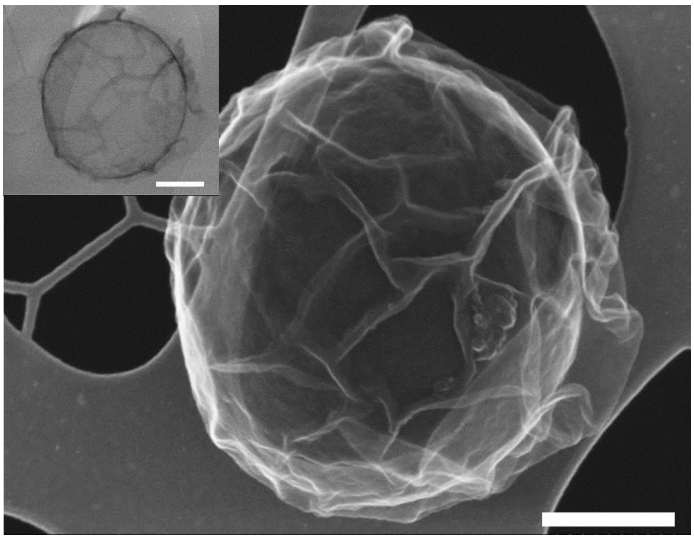

Figure 6.3 The Spherical graphene-based nanosphere. A scanning transmission electron microscopy (STEM) images illustrating spherical features of 3D CGrBs at the injectrion rate of 600 ul/hr which have a hollow structure of few ridges on thin layer (scale bar: 300 nm). The inset of image of the graphene-based sphere to show a hollow structure.

The degree of deformation and the size of 3D CGrSs can be tuned by controlling the injection rate of toluene in O/W emulsion and results for injection rates of 100, 200 and 600 µl/hr are shown in **Figure 6.4**a, b, and c, and the individual particles are presented in **Figure 6.4**d, e, and f, respectively. The size of the crumpled particles range from 200 nm to 1000 nm in diameter at three different injection rates, but are not largely affected by the injection rate of toluene. On the other hand, the degree of deformation producing ridges and vertices increases with decreasing injection rate of toluene from 100 µl/hr to 600 µl/hr. The confinement force to crumple 2D MLGs is dependent on the evaporation rate and the concentration of the dispersed graphene.

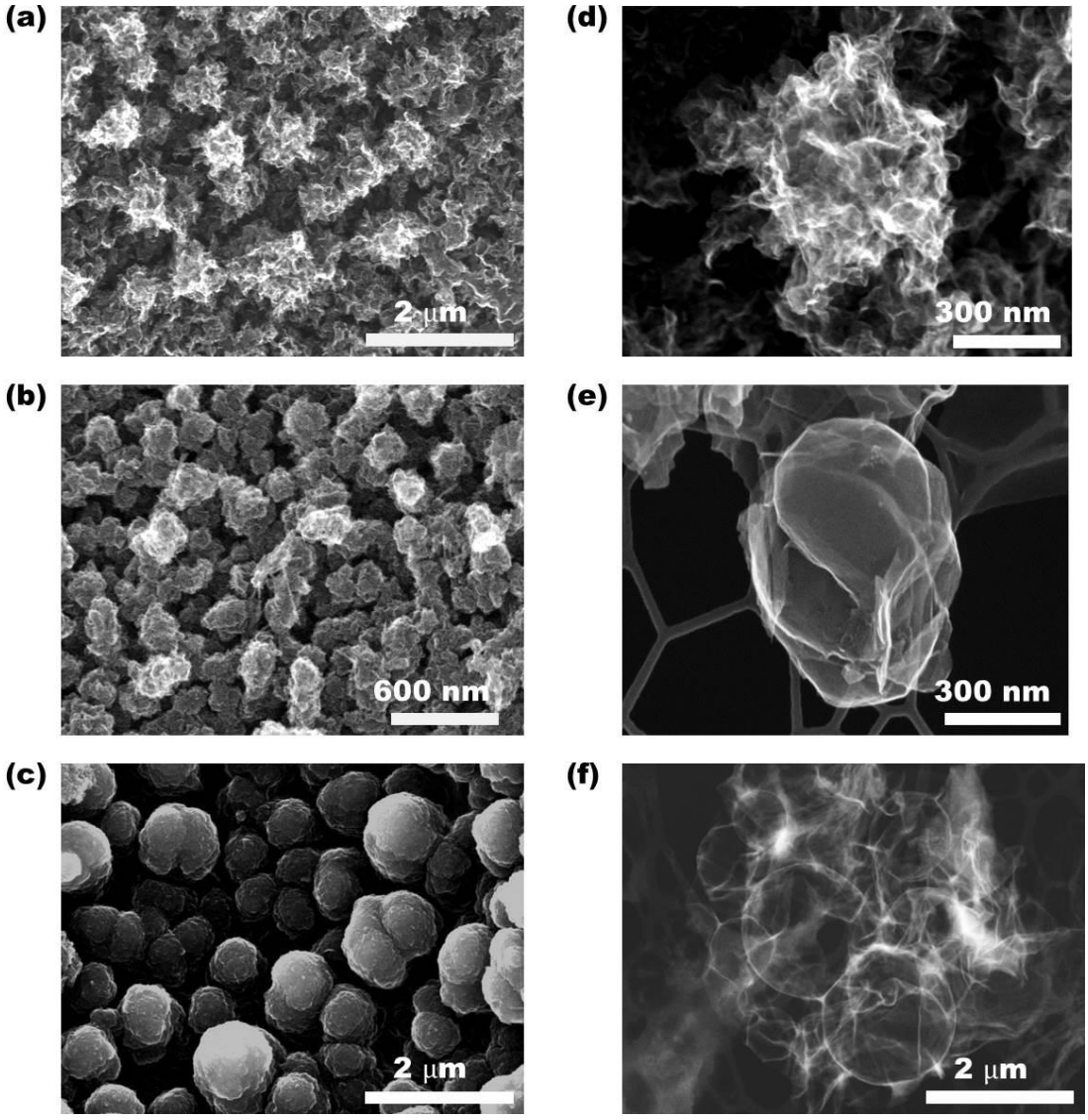

Figure 6.4 STEM images for the crumpled graphene balls corresponding to the rate of the injected toluene into aqueous single reactor arc discharge system. (a), (d) at the rate of 100 ul/hr and its individual particles. (b), (e) at the rate of 200 ul/hr and its individual particles. (c), (f) at the rate of 600 ul/hr and its individual particles. The inset image in (f) shows its hollow structure by transmission mode with STEM. The scale bar shown in each image.

As the 2D graphene sheets overlap during the irreversible deformation, the higher graphene sheet concentration results in thicker graphene flakes leading to larger particles,

which is demonstrated by TEM images at injection rates of 100 µl and 600 µl, respectively. However, the concentration of 2D MLGs produced is maintained at the same level because the applied voltage and current are constant during the arc discharge, which leads the average size to be largely unaffected by the injection rate of toluene. The degree of deformation of the 2D MLGs decreases as the surface area of the individual toluene droplet is increased by the higher injection rate. This is due to the higher concentration of the 2D MLGs at the interface between water and toluene within each droplet. Therefore, the highly crumpled particles can be obtained at lower injection rates. At the higher injection rate (600 µl/hr), particles with thicker graphene layers are formed, making them highly resistant to deformation. These structures were also found to be hollow at the center and contained few ridges on their surface as shown in **Figure 6.4**c and f. The 2D graphene sheets can also be rolled into carbon nanotube structures a few nanometers in diameter without breaking chemical bonds, this irreversible deformation of graphene into 3D crumpled structure was evaluated in terms of the confinement force necessary for plastic deformation.

In further investigating the arc discharge plasma zone, we have found that our particles were largely produced by an exfoliation process unlike conventional arc discharge in water. In our arc discharge process, the temperature will rise up to less than 2000 K at 4 A, which demonstrate that the 2D MLGs are produced by an exfoliation process. This assumption is supported by the observation of very large, kinks and folded structures in the graphene sheets by scanning transmission electron microscope (STEM), as shown in the inset of **Figure 6.3**. These are morphological features commonly observed in exfoliated graphenes.[17]

As we demonstrated, the arc discharge in water generates a plasma zone composed of electrons and O^+, O^{++} and H^+ ions.[20] We assumed that the oxidation occurs during the exfoliation due to the chemical reaction of a few carbon radicals with these reactive species. In order to prove our assumption, X-ray photoelectron spectroscopy (XPS) was performed as a direct means to estimate the number of defects in 2D MLGs, and the 3D CGrSs that were produced with the same condition.

Results for the XPS analysis are shown in **Figure 6.5**. In wide-scan XPS spectra, the peaks appearing at 284.90 eV and 532.90 eV can be assigned to C1s and O1s, respectively, which indicate the oxidation of 2D MLGs and 3D CGrSs during the arc discharge in water, shown in **Figure 6.5**a. High-resolution C1s XPS spectrum for 2D MLGs and 3D CGrSs are shown in **Figure 6.5**b and c. Deconvolution of the spectra for 2D MLGs indicates that the relative content of the non-oxygenated ring C atoms (284.5 eV) was 46.1%, that of C atoms in C-O bonds (285.9 eV) was 34.8%, and that of carboxylate C atoms (O-C=O, 288.15 eV) was 19.1%, shown in **Figure 6.5** b. Moreover, deconvolution of high-resolution C1s spectra for 3D CGrSs indicates that the relative content of the non-oxygenated ring C atoms (284.4 eV) was 58.3%, that of C atoms in C-O bonds (286.2 eV) was 32.2%, and that of carboxylate C atoms (O-C=O, 288.5 eV) was 9.5%, shown in **Figure 6.5**c. Based on the XPS data, the defects in the sample arise from the oxidation by reactive species in the plasma zone, and the relative content of the non-oxygenated ring C atoms is much higher than that of conventional GO obtained using chemical methods.[18,19] Therefore, the chemical composition of the graphitic carbon particles produced by the arc discharge in O/W emulsions are comparable to reduced 2D graphene oxide sheets or 3D graphene particles.

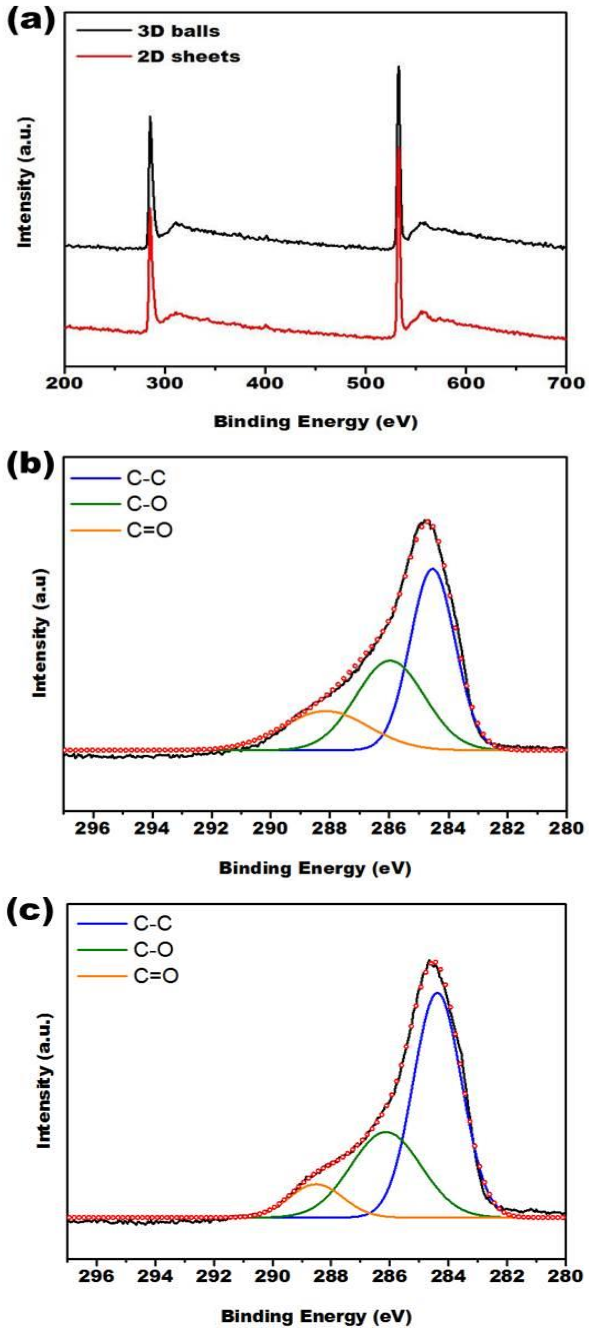

Figure 6.5 X-ray photoemission spectroscopy (XPS). (a) Surface analysis results of 2D MLGs and 3D CGrBs surfaces characterized by using XPS. The top graphs show the XPS survey results of 3D CGrBs on top and 2D MLGs on bottom. (b) High-resolution XPS of the C 1s peak for 2D MLGs. (c) High-resolution XPS of the C 1s peak for 3D CGrBs. (d) Raman spectra of 3D CGrBs (black, top) and 2D MLGs (red, bottom). The ratio of I_D/I_G is 0.12 for 3D CGrBs and 0.13 for 2D MLGs, respectively.

Raman spectroscopy was used to investigate the graphitic carbon structure and quality of the 2D MLGs and the 3D CGrSs. In the Raman spectra shown in **Figure 6.6**, the 2D peaks correspond to the specific stacked number of layers. In the 2D peaks for the 2D MLGs, a peak is observed at 2688 cm^{-1}, which indicates that the exfoliated graphene is stacked less than 10 layers;[22, 23] the intensity at 2660 cm^{-1} indicates a monolayer of graphene, and the peak shift to 2690 cm^{-1} indicates an increase in the number of stacked layers.[23]

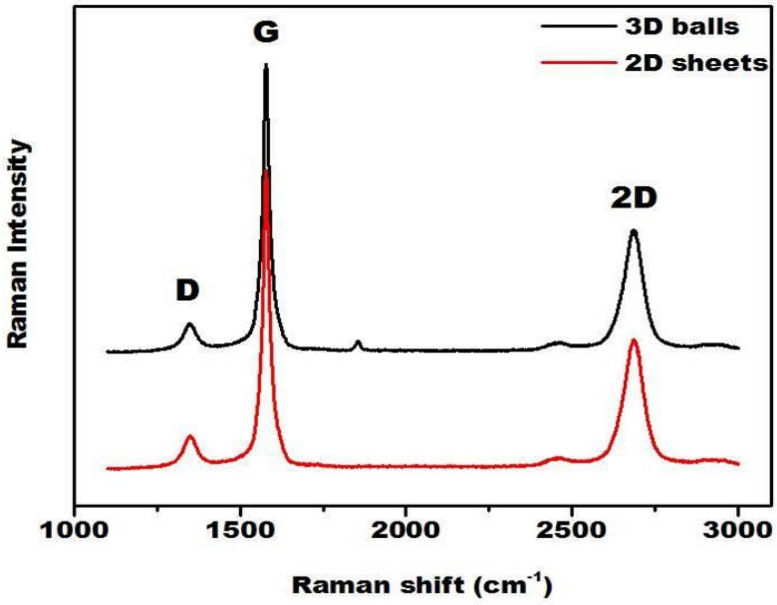

Figure 6.6 Raman Spectra of 3D CGrBs and 2D MLGs. Raman spectra of 3D CGrBs (black, top) and 2D MLGs (red, bottom). The ratio of ID/IG is 0.12 for 3D CGrBs and 0.13 for 2D MLGs, respectively.

The intensity of the D-peak at 1351 cm^{-1} is associated with defects in the graphene. We note that the intensity of the D-peak is significantly smaller than the G-peak at 1578 cm^{-1}, and the ratio of D/G is 0.13. In addition, the 3D CGrSs were also investigated and

the peak positions are not changed. The intensity of the D-peak at 1351 cm^{-1} is still significantly small compared to the G-peak at 1578 cm^{-1}, and though the relative intensity of the D-peak is slightly decreased (D/G ratio = 0.12) compared to the exfoliated graphene sheets, the structural quality from Raman spectroscopy demonstrates that the 2D MLGs and 3D CGrSs retains their unique pristine structure and contain few defects.

In order to investigate the mechanism of 2D MLGs deformation into 3D CGrSs, the number of stacked layers was analyzed by means of atomic force microscopy (AFM). We used atomic force microscopy (AFM) to measure the height that allows the calculation of the number of layers, as shown in **Figure 6.7**. Under the AFM, the graphenes appear to be a very uniform in thickness. The thickness of 2D MLGs was ~4.8 nm, which indicates that the exfoliated graphene are stacked 6 to 7 layers, based on the fact that the thickness of a monolayer of graphene oxide sheets is ~0.7 nm.[18]

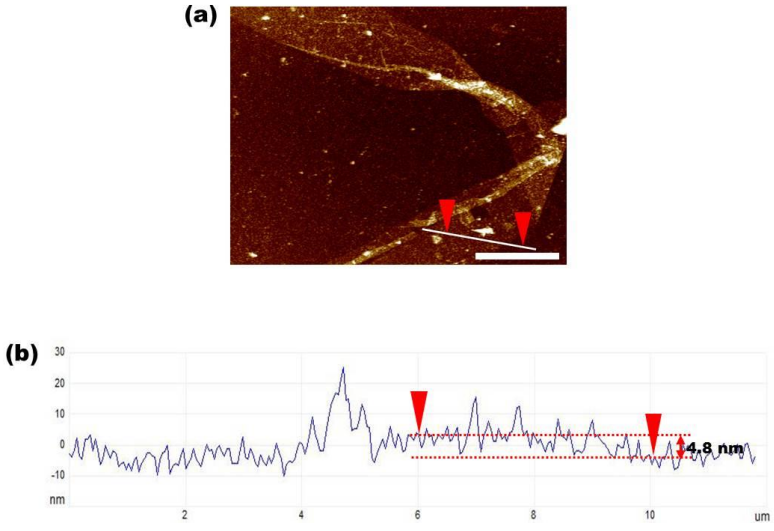

Figure 6.7 Materials Characterization using Atomic force microscopy (AFM): a) Topographical images of the exfoliated 2D MLGs. b) The height profile of the 2D MLGs along the line marked in (a).

For the size distribution of the exfoliated graphene, systematic statistical analysis was performed by the combination of optical microscopy and Raman spectroscopy. Graphene sheets of SiO_2 on Si were observed to be 300 nm thick, as shown in **Figure 6.8**. **Figure 6.8**b shows that the size distribution of the exfoliated multi-layered graphene is $141.5 \pm 13.5\ \mu m^2$.

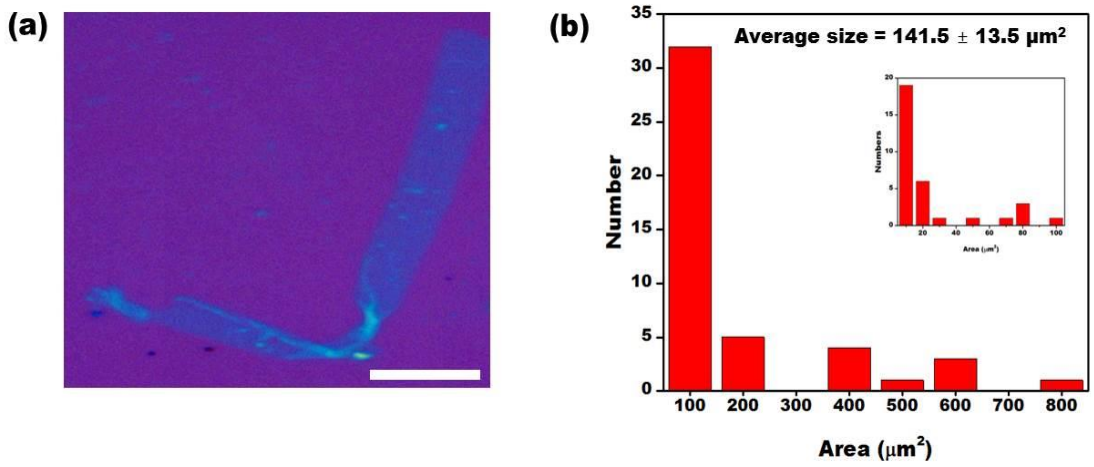

Figure 6.8 Size distribution of the exfoliated graphene for estimation of the crumpling force. (a) Light microscope image of the exfoliated 2D MLGs on SiO_2/Si substrate (SiO_2 thickness: 300 nm). (b) size distribution of the exfoliated 2D MLGs analyzed by Image J from 100 optical images of the 2D MLGs.

The crumpling mechanism and confinement forces involved in 3D CGrSs can be evaluated as non-interacting materials (self-avoidance) such as paper and foils.[10-12,14,15] According to the fractal scaling law, the fractal dimension can be obtained by plotting the calculated mass of 3D CGrSs as a function of the diameter of the resulting particles. The linear relationship of 3D CGrSs mass as a function of diameter for the

entire particles size is presented on a log-log scale in **Figure 6.9**. By fitting the data to Equation (1), the fractal dimension is obtained as D = 2.29 for 3D CGrSs in **Figure 6.9.**

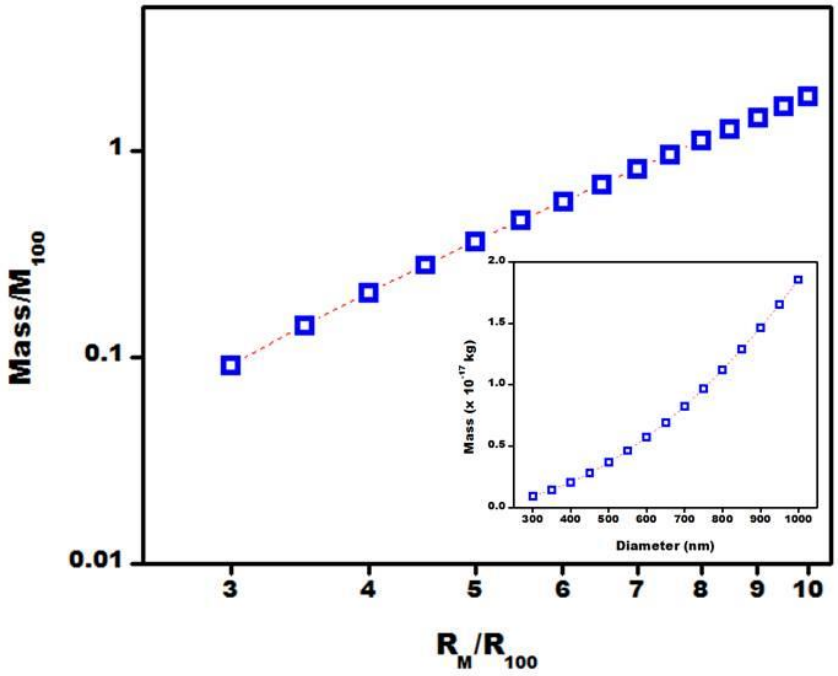

Figure 6.9 Calculated mass of 3D CGrBs as function. The entire particles size range according to the scaling law presented by log-log scale. Data scaled to data at 100 nm. Inset shows 3D CGrBs mass corresponding to their diameter.

The confinement force was also calculated separately with the assumption that the particles shown in Figure 5.4a and Figure 5.4c have a perfect spherical structure with D = 3. The crumpling process is related to the compressive/capillary force produced during toluene evaporation. The confinement force is associated with the Young's modulus and the 2D MLGs thickness by,

$$\rho = \rho_m \left(\frac{F}{Yh}\right)^{\delta D} \left(\frac{R}{h}\right)^{3-D} \qquad (2)$$

where ρ is the mass density of a spherical particle, ρ_m is density of GO (1910 kg/m^3), Y is the two-dimensional Young's modulus, R is the particle radius, h is the sheet thickness (4.8×10^{-9} m for the measured 2D MLGs), D is the measured fractal dimension of GO (2.29), and δ is the force scaling exponent for a non-interacting sheet (0.25).[11] For Y, we used the two-dimensional elastic constant of a single reduced graphene oxide sheet (129 N/m).[24] The density, ρ, is evaluated directly from our mass-diameter measurement.

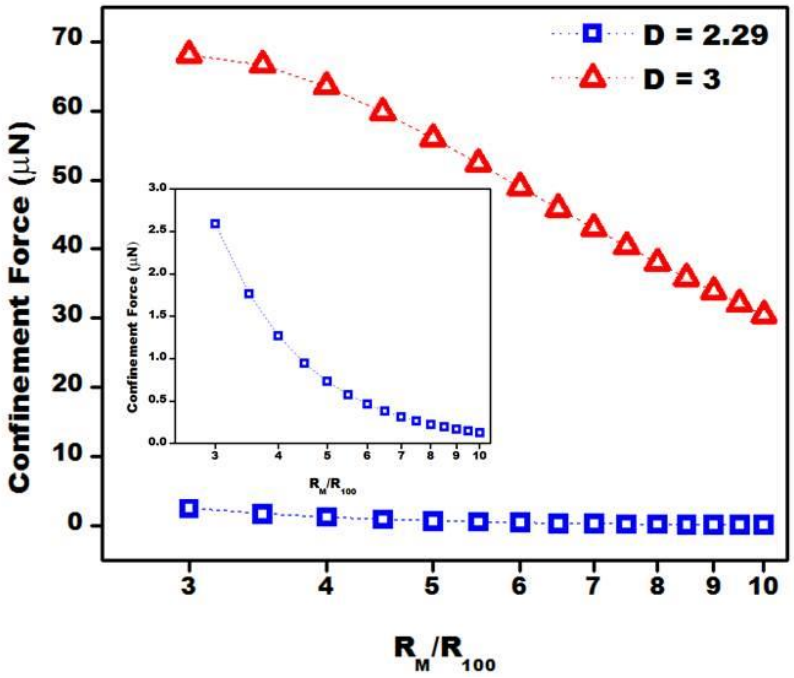

Figure 6.10 Calculation of the confinement force. Geometric mean diameter of 3D CGrBs and the confinement force corresponding to D=3 (top, red) and D=2.29 (bottom, blue), respectively. The confinement force for D = 2.29 is magnified in the inset.

Figure 6.10 shows that the confinement force is around 70 μN for a spherical particles (D = 3) and 2.6 μN for crumpled particles (D = 2.29) in the inset of Figure 5.10,

respectively, which is inversely proportional to diameter of the 3D CGrSs. In the case of crumpled particles (D = 2.29), the size distribution of the exfoliated 2D MLGs ranges from 10 μm (100 μm^2) to 35 μm (1000 μm^2) corresponding to the change in diameter of the 3D CGrSs from 300 nm to 1000 nm. Therefore, the crumpled particles are likely composed of a single sheet or just a few sheets of 2D MLGs as reported in other studies.[12] For the sphere with D = 3, the confinement force was evaluated as shown in Figure 5.10. The confinement force was found to be ~70 μN, a much higher value than for the crumpled particles. The confinement force is proportional to the evaporation rate of the droplets ($F \propto \kappa^{4.72}$).[15]

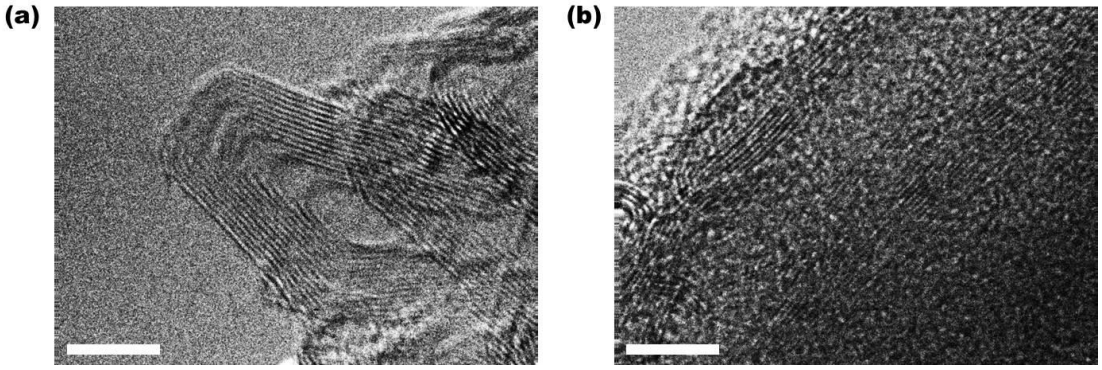

Figure 6.11 The number of stacked graphene layers. TEM images demonstrating the morphology and the thickness of 3D CGrSs at different injection rate. (a) the injection rate of 100 μl/hr and (b) the injection rate of 600 μl/hr (scale bar: 5nm)

In addition, the volume of the toluene droplet increases in surface area, which leads to a higher concentration of graphene at the interface between water and toluene. Increased numbers of layers are formed at the interface, resulting in a higher bending modulus and less deformation. This leads to higher resistance against deformation and

larger particles because the confinement force has the relationship, $F \propto C^{1.57}$.[15] Therefore, the slower evaporation of the toluene droplet and the higher concentration of graphene produce greater compression forces creating spherical particles.

6.4 Conclusion

In conclusion, we have developed a seamless aqueous single reactor arc discharge process in O/W emulsion that produces 2D MLGs which then transition into 3D CGrSs through plastic deformation. Our arc discharge process has three important features: 1) 2D multi-layered graphene is produced by the exfoliation process of the graphite electrodes, wherein the low defects such as bonding with oxygen is comparable to reduced graphene oxide (rGO); 2) the degree of deformation of the 2D MLGs can be tuned by controlling the injected amount of oil (toluene), which leads to the controllable morphological features of the exfoliated 2D MLGs; and 3) the confinement force to crumple 2D MLGs is around 2.5 μN (D = 2.29) and increase to 70 μN for a spherical particles (D = 3). In the future, the crumpled graphene particles may accommodate organic/inorganic nanoparticles for various applications demanding a high specific surface area of graphene.

Chapter 6, in part, is a reprint of the material as it appears Sejung Kim, Youngjun Song, Tsukasa Takahashi, Taeseok Oh, and Michael J. Heller, An aqueous single reactor arc discharge process for the synthesis of graphene nanospheres. The dissertation author

was the primary investigator and author of this material.

6.5 References

1. Zhu, Y., Murali, S., Stoller, M. D., Ganesh, K. J., Cai, W., Ferreira, P. J., Pirkle, A., Wallace, R. M., Cychosz, K. A., Thommes, M., Su, D., Stach, E. A., Ruoff, R. S. *Carbon-based supercapacitors produced by activation of graphene.* Science 2011, **332**: p. 1537-1541.

2. Miller, J. R., Outlaw, R. A., Holloway, B. C. *Graphene double-layer capacitor with ac line-filtering performance.* Science 2010, **329**: p. 1637-1639.

3. Smith, A. J., Chang, Y. –H., Raidongia, K., Chen, T. -Y., Li, L. -J., Huang, J. Adv. Energy Mater. 2014, **4**: p. 1400398; b) Luo, J., Jang, H. D., Huang, J. ACS Nano 2013, **7**: p. 1464.

4. a) Mao, S., Wen, Z., Huang, T., Hou, Y., Chen, J. Envery Environ. Sci. 2014, **7**: p. 609; b) Mao, S., Wen, Z., Kim, H., Lu, G., Hurley, P., Chen, J., ACS Nano 2012, **6**: p. 7505.

5. Stankovich, S., Dikin, D. A., Dommett, G. H. B., Kohlhaas, K. M., Zimney, E. J., Stach, E. A., Piner, R. D., Nguyen, S. T., Ruoff, R. S. Nature 2006, **442**: p. 282.

6. Ramanathan, T., Abdala, A. A., Stankovich, S., Dikin, D. A., Herrera-alonso, M., Piner, R. D., Adamson, D. H., Schniepp, H. C., Chen, X., Ruoff, R. S., Nguyen, S. T., Aksay, I. A., Prud'homme, R. K., Brinson, L. C. Nature Nanotechnol. 2008, **3**: p. 327.

7. a) Zang, J., Ryu, S., Pugno, N., Wang, Q., Tu, Q., Buehler, M. J., Zhao, X. Nature Mater. 2013, **12**: p. 321; b) Zang, J., Cao, C., Feng, Y., Liu, J., Zhao, X. Sci. Reports 2014, **4**: p. 6492.

8. Chen, Y., Guo, F., Jachak, A., Kim, S. -P., Datta, D., Liu, J., Kulaots, I., Vaslet, C., Jang, H. D., Huang, J., Kane, A., Shenoy, V. B., Hurt, R. H. Nano Lett. 2012, **12**: p. 1996.

9. Sohn, K., Na, Y. J., Chang, H., Roh, K. -M., Jang, H. D., Huang, J. Chem. Commun. 2012, **48**: p. 5968.

10. Vliegenthart, F., Gompper, G. Nature Mater. 2006, **5**: p. 216.

11. Balankin, A. S., Silva, I. C., Marinez, O. A., Huerta, O. S. Phys. Rev. E 2007, **75**: p. 051117.

12. Tallinen, T., Astrom, J. A., Timonen, J. Nature Mater. 2009, **8**: p. 25.

13. Luo, J., Jang, H. D., Sun, T., Xiao, L., He, Z., Katsoulidis, A. P., Kanatzidis, M. G., Gibson, J. M., Huang, J. ACS Nano 2011, **5**: p. 8943.

14. Ma, X., Zachariah, M. R., Zangmeister, C. D. Nano Lett. 2012, **12**: p. 486.

15. Wang, W. -N., Jiang, Y., Biswas, P. J. Phys. Chem. Lett. 2012, **3**: p. 3228.

16. Chen, L., Yu, S., Wang, H., Xu, J., Liu, C., Chong, W. H., Chen, H. J. Am. Chem. Soc. 2013, **135**: p. 835.

17. a) Stankovich, S., Dikin, D. A., Piner, R. D., Kohlhaas, K. A., Kleinhammes, A., Jia, Y., Wu, Y., Nguyen, S. T., Ruoff, R. S. Carbon 2007, **45**: p. 1558; b) Zhu, Y., Murali, S., Stoller, M. D., Velamakanni, A., Piner, R. D., Ruoff, R. S. Carbon 2010, **48**: p. 2118.

18. Tung, V. C., Allen, M. J., Yang, Y., Kaner, R. B. Nature Nanotechnol. 2009, **4**: p. 25.

19. a) Sano, N., Wang, H., Chhowalla, M., Alexandrou, I., Amaratunga, G. A. J. Nature 2001, **414**: p. 506; b) Sano, N., Wang, H., Alexandrou, I., Chhowalla, M., Teo, K. B. K., Amaratunga, G. A. J. J. Appl. Phys. 2002, **92**: p. 2783.

20. Eubank, P. T., Pate, M. R., Barrufet, M. A., Bozkurt, B. J. Appl. Phys. 1993, **73**: p. 7900.

21. Nair, R. R., Blake, P., Grigorenko, A. N., Novoselov, K. S., Booth, T. J., Stauber, T., Peres, N. M. R., Geim, A. K. Science 2008, **320**:p. 1308.

22. Hernandez, Y., Nicolosi, V., Lotya, M., Blighe, F. M., Sun, Z., De, S., McGovern, I. T., Holland, B., Byrne, M., Gun'ko, Y. K., Boland, J. J., Niraj, P., Duesberg, G., Krishnamurthy, S., Goodhue, R., Hutchison, J., Scardaci, V., Ferrari, A. C., Coleman, J. N. Nature Nanotechnol. 2008, **3**: p. 563.

23. Shih, C. -J., Vijayarahgavan, A., Krishnan, R., Sharma, R., Han, J. -H., Ham, M. -H., Jin, Z., Lin, S., Paulus, G. L. C., Reuel, N. F., Wang, Q. H., Blankschtein, D., Strano, M. S. Nature Nanotechnol. 2011, **6**: p. 439.

24. Robinson, J. T., Zalalutdinov, M., Baldwin, J. W., Snow, E. S., Wei, Z., Sheehan, P., Houston, B. H. *Wafer-scale reduced graphene oxide films for nanomechanical devices.* Nano Lett. 2008, **8**: p. 3441.

Chapter 7: Conclusions and Future Directions

In this work, we have developed a novel synthetic process to produce a controllable number of graphene layers and an adjustable degree of oxygen-related defects by lowering the arc discharge power during the manufacturing process. In addition, a morphological transition has been achieved with the use of an O/W emulsion.

First, the capability to control the number of graphene layers and the degree of oxidation of graphene has been easily achieved by adjusting the arc discharge power. The conventional arc discharge in water evaporates carbon molecules from the graphite electrodes by using high current, which can heat up to 4000 K (sublimation temperature of graphite), followed by recombination into a specific shape of particles such as carbon onions and carbon nanotubes. However, unlike the conventional arc discharge in water, the graphene is exfoliated from the graphite by heating up to less than 2000 K, which is enough to thermally expand the interlayer distance between graphene followed by water cavitation to induce a mechanical fluctuation in the surface of the graphite. The number of stacked graphene layers can be controlled by lowering the current level down to 1 A, which leads to a reduction in the arc discharge power. At 1 A, the number of graphene layers is 2 to 3 with 78 %. Otherwise, the arc discharge can produce multi-layered graphene (4-7 layers with 78%). The exfoliated graphene has the feasibility to be used as transparent electrodes with high transmittance by transferring graphene films onto a transparent substrate. There is still a need to optimize the production of a monolayer of graphene by adjusting the arc discharge power and the properties of the dielectric medium in a practical scalable way.

Second, the aqueous arc discharge was created by two graphite electrodes used as an anode and cathode using water as the dielectric medium. Conveniently, the water was shown to be an effective collector for the produced graphene and also acted as a coolant to maintain a stable temperature during the process. In addition, the water can be used as a source of ions such as O^{+}, O^{++}, H^{+} in the plasma zone and provides oxygen ions for the oxidation of the graphene. Elemental analysis results demonstrated that the degree of oxidation of graphene can be controlled according to the arc discharge power by forming oxygen-related functional groups on graphene layers. Moreover, the concentration of ions produced by an arc discharge is proportionally increased with power. The controllable degree of oxidation of graphene has been investigated in applications for use as a water desalination membrane. According to the affinity of graphene to water, the graphene-based membranes enhance the salt rejection rate and the water flux across the graphene-based membranes. However, for the application of water desalination, the fabrication process should be modified in order to make a highly smooth graphene-based membrane surface to enhance the salt ion rejection performance and to maximize the water flux.

Lastly, the arc discharge process has been found to be a seamless process for crumpling graphene into graphene-based nanospheres: the use of O/W emulsion systems during the manufacturing process results in the conversion of 2D nanostructures into 3D nanostructures. The hole at the fixed cathode can supply toluene into the arc discharge system and the rate of supplied toluene can be adjusted. The produced graphene can be crumpled from 2D to 3D structures by suppling an oil phase into the process. The graphene can be encapsulated inside oil droplets followed by the evaporation of oil. The degree of crumpling can be controlled according to the amount of toluene supplied into

the system and the confinement force can be calculated in the range up to 70 μN for graphene-based nanospheres. Furthermore, this seamless arc discharge process can produce graphene-based composite particles with other various nanoparticles such as silicon nanoparticles, and metal/metal oxide nanoparticles. Beyond this effective synthetic process, the arc discharge can be developed in a more effective and scalable way to produce high quality graphene and their composite particles.